HYBRID FRP-CONCRETE BRIDGE DECK SYSTEMS
Project No.: C-02-07

FINAL REPORT II:
LONG TERM PERFORMANCE OF HYBRID FRP-CONCRETE BRIDGE DECK SYSTEM

Amjad J. Aref, Ph. D.
Professor
Department of Civil, Structural and Environmental Engineering
University at Buffalo-State University of New York
Buffalo, NY, 14260

and

Gordon Warn, Ph.D.
Assistant Professor
Department of Civil and Environmental Engineering
The Pennsylvania State University

October 2009

DISCLAIMER

This report was funded in part through grant(s) from the Federal Highway Administration, United States Department of Transportation, under the State Planning and Research Program, Section 505 of Title 23, U.S. Code. The contents of this report do not necessarily reflect the official views or policy of the United States Department of Transportation, the Federal Highway Administration or the New York State Department of Transportation. This report does not constitute a standard, specification, regulation, product endorsement, or an endorsement of manufacturers.

1. Report No. C-02-07	2. Government Accession No.	3. Recipient's Catalog No.	
4. Title and Subtitle HYBRID FRP-CONCRETE BRIDGE DECK SYSTEM REPORT II: LONG TERM PERFORMANCE OF HYBRID FRP-CONCRETE BRIDGE DECK SYSTEM		5. Report Date June 2009	
		6. Performing Organization Code:	
7. Author(s) Amjad J. Aref and Gordon Warn		8. Performing Organization Report No.	
9. Performing Organization Name and Address State University of New York at Buffalo 212 Ketter Hall – Buffalo – NY - 14260		10. Work Unit No. (TRAIS)	
		11. Contract or Grant No.	
12. Sponsoring Agency Name and Address NYS Department of Transportation 50 Wolf Road Albany, New York 12232		13. Type of Report and Period Covered Final Report	
		14. Sponsoring Agency Code	
15. Supplementary Notes Project funded in part with funds from the Federal Highway administration			
16. Abstract This report describes the investigation of the long term structural performance of a hybrid FRP-concrete (HFRPC) bridge deck on steel girders. The study aimed at assessing three long term aspects pertaining to the HFRPC bridge deck: (1) creep characteristics, (2) fatigue performance, and (3) ultimate capacity. ..			
17. Key Words FRP Composites, Hybrid Design, Bridge Deck, Concrete, Bridge Superstructure	18. Distribution Statement No restrictions		
19. Security Classification (of this report) Unclassified	20. Security Classification (of this page) Unclassified	21. No of Pages 72	22. Price

TABLE OF CONTENTS

Page

Page

Page

EXECUTIVE SUMMARY

This report describes the investigation of the long term structural performance of a hybrid FRP-concrete (HFRPC) bridge deck on steel girders. The study aimed at assessing three long term aspects pertaining to the HFRPC bridge deck: (1) creep characteristics, (2) fatigue performance, and (3) ultimate capacity. In achieving these objectives, a series of laboratory testing was conducted on a scaled HFRPC deck that is compositely connected to steel girders by clusters of shear studs. The experimental results revealed that the structural performance of the hybrid FRP-concrete bridge deck was according to the design expectations and meets AASHTO specifications. Most notably, the specimen showed no stiffness degradation after more than two million cycles of fatigue loading. Moreover, after completing two million cycles of fatigue loading the HFRPC deck sustained 2.7 times the Tandem load without damage. The ultimate capacity of the deck was found to be six times the Tandem load.

ACKNOWELEDGENTS

The work described in this report was funded by New York State Department of Transportation (NYSDOT) through grant C-02-07 administered by Transportation Infrastructure Research Consortium (TIRC). The original concept of the HFRPC bridge deck was partly developed by Dr. Wael Alnahhal in his Ph.D. Dissertation, We would like to thank him for supplying the information that eased the execution of the project. The authors also thank Dr. Sreenivas Alampalli for his guidance and input to this project.

The authors would also like to thank the staff of the Structural Engineering and Earthquake Simulation Laboratory at the State University of New York at Buffalo for their assistance with the setup and execution of each of the testing phases. Finally, special thanks to Scot Weinreber whose expertise and efforts were especially critical in the successful completion of the fatigue testing portion of this study.

SECTION 1

INTRODUCTION

1.1 General

The United States (U.S.) has one of the largest highway networks in the world. The efficiency and safety of this network plays an essential role in the continued economic health of the country. The total number of bridges in the U. S. as of 2003 is 615,718 (National Bridge Inventory (NBI), 2003), and nearly 26.3 percent of these bridges are either structurally deficient or functionally obsolete (FHWA 2003). There is, however, a major challenge to reduce or eliminate deficient structures. A solution to this challenge may be to use new materials or to implement new structural systems. Among new structural materials, fiber reinforced polymers (FRP) composites have continued to play an important role in solving some of the persistent problems in infrastructure applications due to their superior material properties such as high specific stiffness, high specific strength, high corrosion resistance, light weight, and durability.

Based on these advantages and a wide variety of practical applications, the composites industry has grown approximately 460% over the past 30 years, from 360,000 tons in 1970 to 1.68 million tons in 2000 (Busel 2000). In spite of all these advantages, FRP composites have higher initial costs than conventional materials used in infrastructure application. To overcome this obstacle and to make the best use of materials, combinations of FRP and conventional materials have recently been investigated by a number of researchers. The advantages of hybrid structural systems include the cost effectiveness and the ability to optimize the cross section based on material properties of each component.

According to Mirmiran (2001), the most effective use of FRP composites is in the form of hybrid construction with concrete, where FRP acts as a load carrying constituent and a protective measure for concrete. Seible et al. (1998) investigated a two span bridge with light weight concrete filled circular CFRP composite tubes. Their preliminary estimates indicate that two different bridge systems (the concrete filled CFRP beams with

reinforced concrete (RC) deck and the concrete filled CFRP beams with pultruded modular E-glass deck) are 20 % and 100 % more expensive, respectively, when compared to a conventional RC slab bridge.

Bridge deck represents a vital component in a bridge system and its durability impacts the overall structural health of a bridge system. Since the US has one of the most extensive highway system in the world and the US bridge inventory well over 600,000 bridges, the long term behavior of bridge decks is a key component in the life cycle cost of bridges in this country. A cursory look at the US bridge inventory reveals that the majority of bridge decks are made of reinforced concrete and many bridge decks often deteriorate at a rapid rate in harsh operational environments. The rapid deterioration of the deck often impacts other critical components of the bridge. Therefore, there is a need to examine new materials and innovative designs using advanced materials. In this study, the long term behavior of the previously developed hybrid FRP-Concrete (HFRPC) bridge deck system that is compositely connected to steel girders by clusters of shear studs is investigated.

1.2 Experimental Setup

In a previous report entitled “Hybrid FRP-Concrete Bridge Deck Systems: Development and System Performance Validation”, Aref and Alnahhal (2006) presented a detailed description of the analysis and design optimization procedures utilized to develop a hybrid FRP-concrete bridge deck system. Along with the analytical studies and system development, the report describes tests that were performed on the bridge models to assess the performance under service load conditions.

In a subsequent amendment to the project, this report describes the work done in assessing the structural long term behavior of the HFRPC bridge deck system. The focus of this study is primarily on long term behavior aspects and assessment of ultimate strength behavior of the HFRPC bridge system. This report describes in detail the experimental study and the findings of the research tasks.

1.3 Research Objectives

The primary objective of this study is to examine the long term behavior of a HFRPC deck system installed on steel bridge girders. In particular, an experimental program was conducted that focused on the following:

1. evaluating the creep characteristics of the HFRPC system;
2. evaluating the fatigue and composite action behavior of HFRPC with steel girders;
3. evaluating the ultimate capacity of the HFRPC deck that is compositely connected to steel girders.

1.4 Report Organization

This report is comprised of six sections. Section two describes the HFRPC deck and steel bridge system. Section three and four describe the Creep and Fatigue experimental program and observed behavior of the bridge system, respectively. Section five presents the destructive experimental testing program aiming at assessing the ultimate capacity of the HFRPC bridge deck bridge system. The conclusions and observations on the long term behavior and ultimate capacity are delineated in section 6. A list of References is provided at the end of this report.

SECTION 2

DESCRIPTION OF STRUCTURAL SYSTEM

2.1 General

In a previous report entitled "Hybrid FRP-Concrete Bridge Deck Systems: Development and System Performance Validation", Aref and Alnahhal (2006) presented a detailed description of the analysis and design optimization procedures utilized to develop a hybrid FRP-concrete (HFRPC) bridge deck system. This section provides a description of the HFRPC bridge deck system that was developed in the previous studies and the experimental model used in the long term structural performance investigation.

2.2 Previous Studies

2.2.1 Hybrid FRP-Concrete Bridge Deck System

The hybrid deck system proposed in the previous study (Aref and Alnahhal 2006; Alnahhal et al. 2008) consists of trapezoidal cell units surrounded by an outer shell forming an integral bridge deck (see Figs. 2.1 and 2.2). A thin layer of concrete was placed in the compression zone of the section that is confined by glass fiber reinforced polymer (GFRP) laminates that enhances the stiffness of the deck, reduces the local deformation of the top surface of the bridge under concentrated load and protects the concrete from the environmental exposure. One of the most likely uses of the proposed hybrid FRP-concrete bridge system is for bridge decks over steel or concrete girders. In this application, the hybrid deck takes the place of traditional steel reinforced concrete decks. To be efficiently used in modern bridge decking application, the proposed hybrid deck must be made to act compositely with steel girders. Thus, a sufficiently robust shear transfer interface at the hybrid deck to steel transition zone is required. In the previous study, welded shear studs were used to connect the hybrid deck to steel girders.

According to Ashby (1991), thin walled box sections represent the most efficient structural forms for beams. Trapezoidal box sections with an inclination angle impart reduced shear stresses at the interface of adjacent box sections. According to Kitane and Aref (2004), the inclination of 3/8 has the smallest deformation at the riding surface. Thus, an inclination of 3/8 was chosen for

the proposed bridge deck system. To evaluate the efficiency of the proposed bridge deck system, a prototype bridge system (6.5 m long and 4.06 m wide) was designed as a simply supported steel bridge with a hybrid FRP-concrete deck. The height of the hybrid deck was limited to 200 mm so that the proposed deck can be used for deck renewal projects. This proposed bridge system has several inherent advantages over an all-composite bridge, which can be summarized in the following points:

- GFRP is corrosion-resistant and the concrete is protected from any potential harsh environmental exposure; thus, the system will require less maintenance than conventional bridges.
- Concrete is designed to always be in compression in the longitudinal direction. The fact that concrete is not used in the tension side leads to significant weight reduction when compared to a concrete-filled FRP section. Moreover, the encasement of concrete prevents cracking and thus mitigation of corrosive elements.
- It has been reported that the local deformation under concentrated point loads resulting from truck wheels may become large for all-composite bridge decks (Bakeri and Sunder1990; Aref 1997). A layer of concrete can effectively reduce this local deformation of the top flange and improve the serviceability of the wearing surface

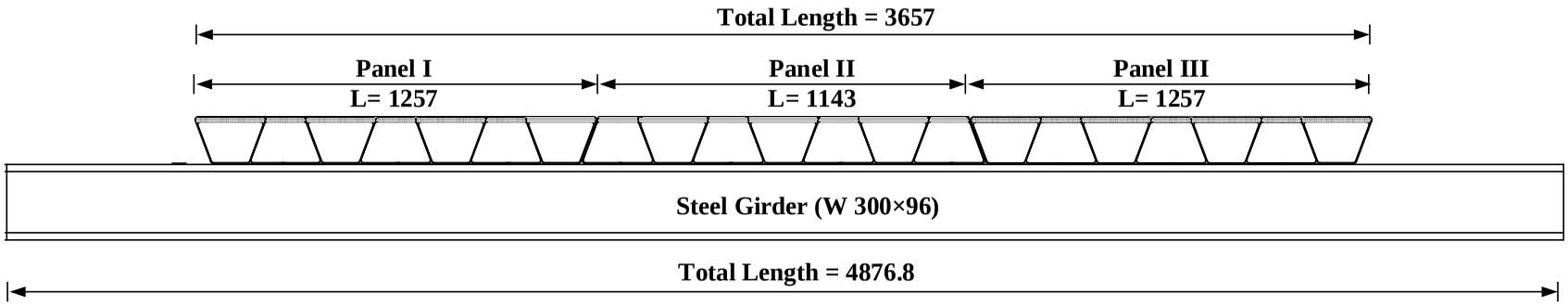

a. Elevation

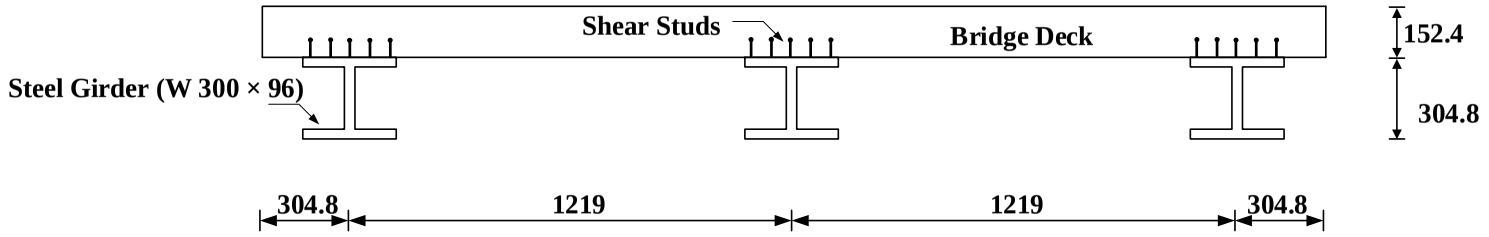

b. Side View

Fig. 2.1 3/4 Scale Model of Steel Bridge with a Hybrid FRP-Concrete Bridge Deck (units in mm)

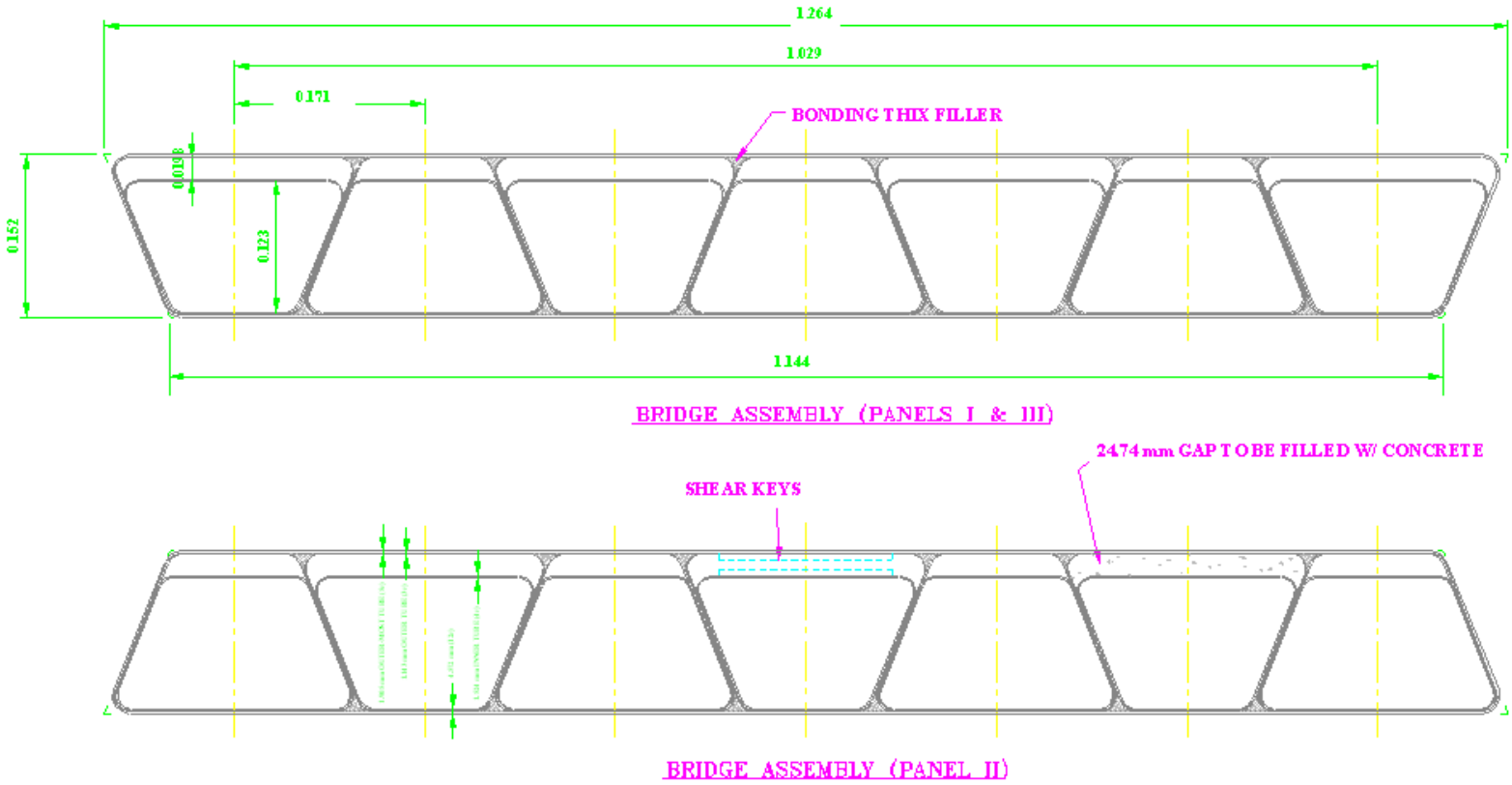

Fig. 2.2 Cross Section of the 3/4 Scale Model of a Hybrid FRP-Concrete Bridge Deck Panels (units in mm)

2.3 Test Specimen

For assessing the long term structural performance of the HFRPC bridge deck system, a test specimen was utilized that represented a 3/4 scale model of a 6.5 m prototype steel bridge. The model had an overall length of 4.88 m and a span length of 4.83m (see Figs. 2.1 and 2.2). The deck model supported on steel girders had a length of 3.05 m, a width of 3.66 m, and a depth of 150 mm. The hybrid FRP-concrete deck specimen (FRP part only) was fabricated at An-Cor Industrial Plastics, Inc., N. Tonawanda, NY. Illustrations of both the elevation and side views of the steel bridge with the hybrid FRP-concrete deck are presented in Fig. 2.1.

The hybrid bridge deck was comprised of three deck panels. Each panel was comprised of seven trapezoidal cross-sections surrounded by an outer shell as shown in Fig. 2.2. A thin layer of concrete was placed in the compression zone of each section. Each trapezoidal section consisted of two layers of laminates (Glass fibers and vinyl ester matrix): the inner tube laminate and the outer tube laminate. The inner tube with glass fiber orientations of $[0^o{}_4]$, was first constructed, and the outer tube was then laminated over the inner tube laminate with a laminate construction $[0^o{}_3]$. The outermost laminate stacking sequence was $[0^o{}_5]$. Table 2.1 shows the stacking sequence and thickness of various components of the bridge deck model. As mentioned above, the stacking sequence chosen for all laminates was $\mathbf{0}^o$. This selection was made because the woven fabric type chosen as reinforcement in this study has almost the same mechanical properties in the two orthogonal directions.

Table 2.1 Thickness and Stacking Sequence of the Hybrid Deck Model

	Stacking Sequence	Thickness (mm)
Inner Tube Laminate	$[0^o{}_4]$	1.524
Outer Tube Laminate	$[0^o{}_3]$	1.143
Outer- Most Tube Laminate	$[0^o{}_5]$	1.905

Each trapezoidal box section was fabricated individually by the hand lay-up process. Consequently, the seven trapezoidal sections were then assembled by using the vacuum bag process. A layer of glass fiber chopped strand mat wetted with vinyl ester resin was applied between box sections to enhance the bonding at the interface between the sections and to allow for a better bond if there exists mismatch between the surfaces being bonded. The seven trapezoidal sections were then wrapped with the outer-most laminate to form the integral deck unit.

To achieve good composite action between GFRP laminates and concrete, shear keys, were installed in staggered positions at the interface of the GFRP laminates and concrete. Each shear key had a length of 0.155 m for the side trapezoidal section and 0.076 m for the middle trapezoidal section in the transverse direction to effectively transfer the shear stress across the concrete-FRP interface. The shear keys were installed on the top surface of the inner tube laminate and on the bottom surface of the outer tube laminate with an interval of 0.508 m. These shear keys were also made of GFRP composites.

The final stage of constructing the deck panels entails the placement of the concrete layer in the cavity allocated during the lamination process. The concrete was poured at the Structural Engineering and Earthquake Simulation Laboratory at University at Buffalo. Foam dams were firstly placed in the shear studs holes (see Fig. 2.3) to avoid leaking of concrete. The cavities were filled completely with concrete. Mechanical properties of both GFRP composites and concrete used in this study (Alnahhal 2007), are listed in Table 2.2 and Table 2.3, respectively.

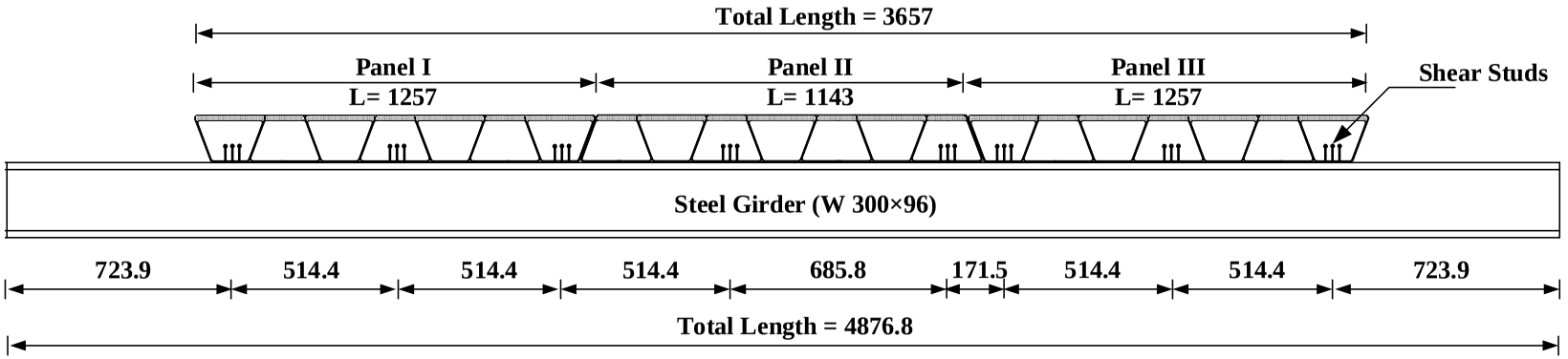

a. Elevation

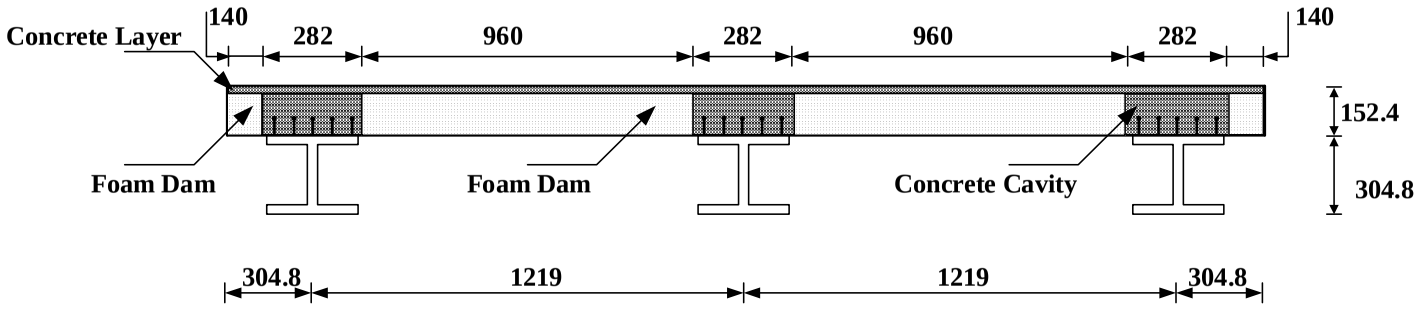

b. Cross Section

Fig. 2.3 Shear Stud Configuration (units in mm)

Table 2.2 Tensile Properties of GFRP

Direction	Coupon	Modulus of Elasticity (GPa)	Tensile Strength (MPa)	Ultimate Strain
Fill	Fill-1	16.38	339.64	0.0267
	Fill-2	16.02	339.64	0.0267
	Fill-3	16.21	339.50	0.0267
	Average	**16.20**	**339.57**	**0.0267**
Warp	Warp-1	15.48	299.72	0.0262
	Warp-2	16.19	285.44	0.0232
	Warp-3	15.96	293.30	0.0255
	Average	**15.88**	**292.82**	**0.0250**

Table 2.3 Mechanical Properties of Concrete

Specimen	Strength f_c' [MPa]	Chord Modulus of Elasticity [GPa]
Sp-1	57.10	31.43
Sp-2	57.20	31.90
Sp-3	52.60	28.30
Average	**55.63**	**30.50**

As seen in Fig. 2.1, the hybrid FRP deck was connected to a typical steel bridge superstructure. The bridge superstructure consisted of three W-beam girders (W300×96). The girders were spaced at 1.22 m center-to-center, and the deck overhang was 0.305 m for the exterior girders. Cross-bracing was placed within the specimen portion of the bridge at 0.25L, 0.5L, 0.75L (where *L* is the span length of the bridge specimen equal to 4.83 m) and at the ends for stability

considerations. The cross-bracing was constructed from L76x76x9.5 (Standard US: L3x3x3/8) stock and welded in place in an 'X' configuration. Cold rolled bars, milled 6.4 mm off the top to ease in welding to the bottom side of the bottom flange, were connected to the girders to act as supports. The end supports, intended to idealize roller supports, were placed on stainless steel plates.

2.3.1 Joining Technique for the Hybrid Deck System

Effective joining techniques represent one of the challenges facing the use of FRP decks. There is limited literature available that discusses connection techniques for many types of decks and the proposed deck is no exception. It is well recognized that component-to-component connection, panel-to-panel connection, and deck-to-support system connection represent some of the most outstanding obstacles that require careful investigation to improve the acceptance of FRP's in bridge construction. Zhou and Keller (2005) documented the technical background, development and design guidelines of FRP bridge deck connections, and design principles concerning the joining of FRP decks. Joining techniques pertaining to panel-to-panel connections and deck-to-support connections for the proposed hybrid deck are discussed in the following subsections.

2.3.1.1 Panel-to-Panel Connections

Panel level connections are necessary to efficiently transfer bending moment and shear forces between jointed panels, provide resistance to dynamic loads, and ensure deformation compatibility. Panel-level connection techniques include—adhesive bonding and mechanical fixing. Mechanical fixing includes shear keys, splicing tongue–groove connections, and clip-joints. Mechanical fixing has the advantage of easy assembly. However, load transfer and failure resistant capability of mechanical fixing is not as efficient as bonded joints (Zhou and Keller 2005). Results from constructed projects with shear key connection show that cracks appeared after a period of exposure to highway vehicle loadings (Reising et al. 2004). The cracking at the shear key connection region shows that mechanically fixed connections are not reliable to resist dynamic vehicle loadings. Zetterberg et al. (2001) proposed two different joining techniques for pultruded composite profiles for bridge deck applications. They used both adhesively bonded

and bolted joints for panel-to-panel connections. Their analytical results showed that the bonded joint is likely to always be easier to design and will be more amendable for realization.

For the proposed system of Aref and Alnahhal (2006), adhesively bonded connections were used to maintain the integrity of the panel-to-panel connection. By using a detailed finite element model [see Alnahhal (2007) for more details], it was found that the maximum transverse shear stress at the interface between adjacent panels of the proposed hybrid deck was 5.44 MPa under service loads (1×Tandem Load) that is smaller than the shear strength of commercially available resin, which ranges from 10.35 to 34.5 MPa (Aref 1997). However, the main disadvantage of bonded connections is the difficulty of disassembly when the panels need repair.

2.3.1.2 Connection of Hybrid Deck on Steel Girders

For system-level connections, shear transfer and connection constructability are the major issues that were addressed in the Aref and Alnahhal study (2006). One of the challenges with the proposed hybrid deck is the development of a reliable connection between the deck and the girders. To date there is a limited number of FRP bridges built world-wide constructed compositely with steel girders. Alternatively, considerable number of FRP decks constructed in the last decade were designed and constructed without accounting for any composite action with the supporting steel girders. The degree of composite action significantly affects the behavior of the composite section of the bridge. If there is no composite action and the section is subjected to some arbitrary vertical loading, the bottom surface of the deck is in tension whereas the top surface of the beam is in compression. Slip occurs between the two surfaces. If partial composite action exists, the slippage will be reduced. However, full composite action is often desired where there will be no slip. One of the issues to be addressed is when an FRP deck replaces a concrete deck in which the bridge original design calls for concrete-steel composite action. While the FRP is much lighter than its counterpart concrete deck, the mere weight reduction resulting from the FRP deck is not likely to offset the increased stresses in the supporting steel that was originally designed and proportioned as composite section with concrete deck. Therefore, there is a need to have FRP decks act compositely with the supporting steel girders.

Mechanical fixing, adhesive bonding, and hybrid joints have been used to connect FRP decks to steel girders. Mechanical fixings include stud-type connections, clamped connections and bolted

connections. Depending on the requirements of a specific project, the deck-girder connection could be a permanent joint with composite action, or an easily constructed connection that provides no composite action between the deck and its supports such as clamped connection detail. In a case where composite action is required, the efficiency of shear transfer and constructability are major factors influencing the design of the connection.

Headed shear studs are routinely used to provide shear continuity across the steel- concrete interface in of steel-concrete composite beams in buildings and bridges. Creative Pultrusions, Inc., Martin Marietta Composites (MMC), and Hardcore Composites (HC) are three manufacturers of FRP bridge decks that have used shear-stud type connections (Market Development Alliance 2000 and Lesko 2001). Moon et al. (2002) investigated three different shear studs connections between steel girders and the MMC Gen4 FRP deck through static and fatigue testing. Static test results suggested that a larger volume of concrete surrounding the shear studs decreased the stress concentration directly behind the shear studs and alleviated local crushing. Moon et al. concluded that approximately 60–70% of the capacity of a longitudinal connection in a continuous concrete deck was developed with this connection. This decreased capacity was due to failure modes related to the discrete nature of FRP decks. Righman et al. (2004) proposed a clamped shear stud connector for FRP decks to steel stringers. Their connection consisted of a threaded shear stud welded to the top flange of the supporting girder and housed inside steel sleeves that were installed within a hole drilled through the FRP deck. The performance of their connector was verified through experimental testing of a reduced scale bridge. Reising et al. (2004) summarized installation issues for four FRP panel systems installed in a 207 m, five-span, and three-lane bridge. All panels were delivered to the site with pre-drilled stud at 1.2 m intervals; 18 cm studs were welded onto the girders through the stud holes. By monitoring the response of the bridge over a period of two years, they observed that the thermal characteristics of the FRP panels, which resulted in unexpected uplifts and significant thermal gradient, are mainly responsible of the vertical displacement of the panels related to the girders.

The proposed hybrid deck of Aref and Alnahhal (2006), that was tested in this study, should serve as a transverse load-carrying element as top chord in composite bridge. After considering the performance and installation issues for various connections, , the proposed bridge deck system of Aref and Alnahhal (2006) was designed and fabricated with welded shear stud

connection that were judged to be the most efficient for an enhanced system-level performance. Construction of this connection for the HFRPC bridge system tested in this study involved: welding the threaded studs to the girder in clusters to avoid excessive drilling in the deck. Then, 0.05 m diameter holes were drilled at each cluster of studs through the top and inner flange of the hybrid specimen for concrete pouring. In addition, rectangular with semi-circle holes were drilled through the bottom face of the specimen. The holes were then blocked off with foam inserts. Subsequently the hybrid deck was placed on the girders. Holes were then filled with non-shrink concrete and covered with the FRP cutouts by using adhesive resin to protect the cutout region.

AASHTO LRFD (1998) has design specification for shear studs for only concrete decks. FEA was used in the Aref and Alnahhal (2006) study to design the shear studs. The averaged horizontal shear force between the hybrid deck and the steel girders was used to determine the number of shear studs required to resist the shear demand. This resulted in, eight (12.7 mm) diameter, (101.6 mm) height stud connectors distributed in certain locations along the entire span. Longitudinal shear studs spacing is specified in Fig. 2.3. The shear studs connectors were intended to provide composite action between the hybrid deck and steel girders to: (1) significantly increase the overall stiffness and load resistance capability of the hybrid bridge system in comparison to its individual girders; (2) improve the ductility of the overall bridge system beyond that of the brittle hybrid deck by engaging the girders, that are made from ductile steel material.

SECTION 3

CREEP TESTING

3.1 General

The creep behavior of the HFRPC (Hybrid FRP-Concrete) system was investigated by monitoring vertical displacements at several locations while the specimen was subjected to a sustained load of 114 kN for a period of 51 days. After 51 days the 114 kN load was removed and the vertical displacements continued to be monitored for an additional 22 days to capture the recovery of the HFRPC system. Provided herein are details of the experimental setup, instrumentation, and experimental results for the investigation of the creep behavior of the HFRPC system.

3.2 Test Setup

The test setup consisted of the HFRPC specimen (including HFRPC deck and steel girders), two W760x284 support beams, four 383 mm by 290 mm steel plates with bonded rubber pads and three steel "load" plates each measuring, approximately, 3000 mm long by 2000 mm wide and 90 mm thick. Figure 3.1 presents a schematic of the elevation view of the HFRPC creep test setup. Each steel plate weighted approximately 38 kN providing a total load of 114 kN that was intended to represent the scaled design tandem load of 124 kN (Alnahhal 2007). The three steel plates were stacked atop four steel-rubber pads on the HFRPC deck each pad intended to simulate the area of a scaled truck tire. Each steel-rubber pad consisted of a steel plate 25 mm thick bonded to a rubber pad 12.5 mm thick each with plan dimensions of 383 mm by 290 mm and arranged in a two-axle truck configurations with 0.9 m between each axle and a with of 1.35 m.

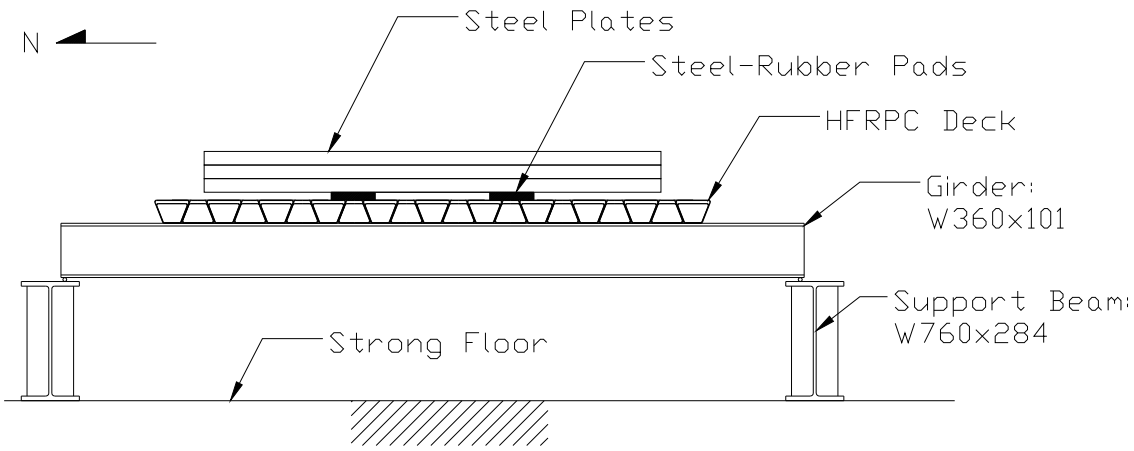

Fig. 3.1 Elevation view of creep test setup

3.3 Instrumentation and Data Acquisition

Instrumentation for the creep test consisted of eight ±50 mm Linear Variable Displacement Transducers (LVDT) and two thermocouples. The LVDTs were used to measure vertical displacement of the HFRPC deck and steel girders and the thermocouples used to measure the ambient temperature above and below the HFRPC deck. Figure 3.2 presents an instrumentation layout shown on a plan view of the HFRPC system including relevant dimensions. Displacement transducers D2, D4, D7 and D8 were attached to the underside of the HFRPC deck at the location of the steel-rubber pads (also the points of loading) whereas D1, D3, D5 and D6 were attached to the steel girders (W360x101) at various locations. Table 3.1 presents a list of instruments including type, range and a brief description of the location of the individual instruments.

Data was collected continuously during loading and unloading of the HFRPC specimen at a sample rate of 5 samples per second although not presented in this report. For the 73 day duration of the test, 51 days with the structure loaded and 22 days after the load was removed, data was collected daily for approximately 30 seconds at a sample rate of 5 samples per second. The average value of the daily data sample was calculated and utilized for the purpose of reporting.

Table 3.1 List of Instruments

ID	Type	Range	Location
D1	LVDT	±50 mm	Top of center girder at south support
D2	LVDT	±50 mm	Bottom of HFRPC at south-west point of loading
D3	LVDT	±50 mm	Bottom of center girder at south line of loading
D4	LVDT	±50 mm	Bottom of HFRPC at south-east point of loading
D5	LVDT	±50 mm	Bottom of west girder at center of span
D6	LVDT	±50 mm	Bottom of center girder at center of span
D7	LVDT	±50 mm	Bottom of HFRPC at north-west point of loading
D8	LVDT	±50 mm	Bottom of HFRPC at north-east point of loading
TH1	Thermocouple	n.a.	Top HFRPC surface at south-east point of loading
TH2	Thermocouple	n.a.	Bottom HFRPC surface at south-east point of loading

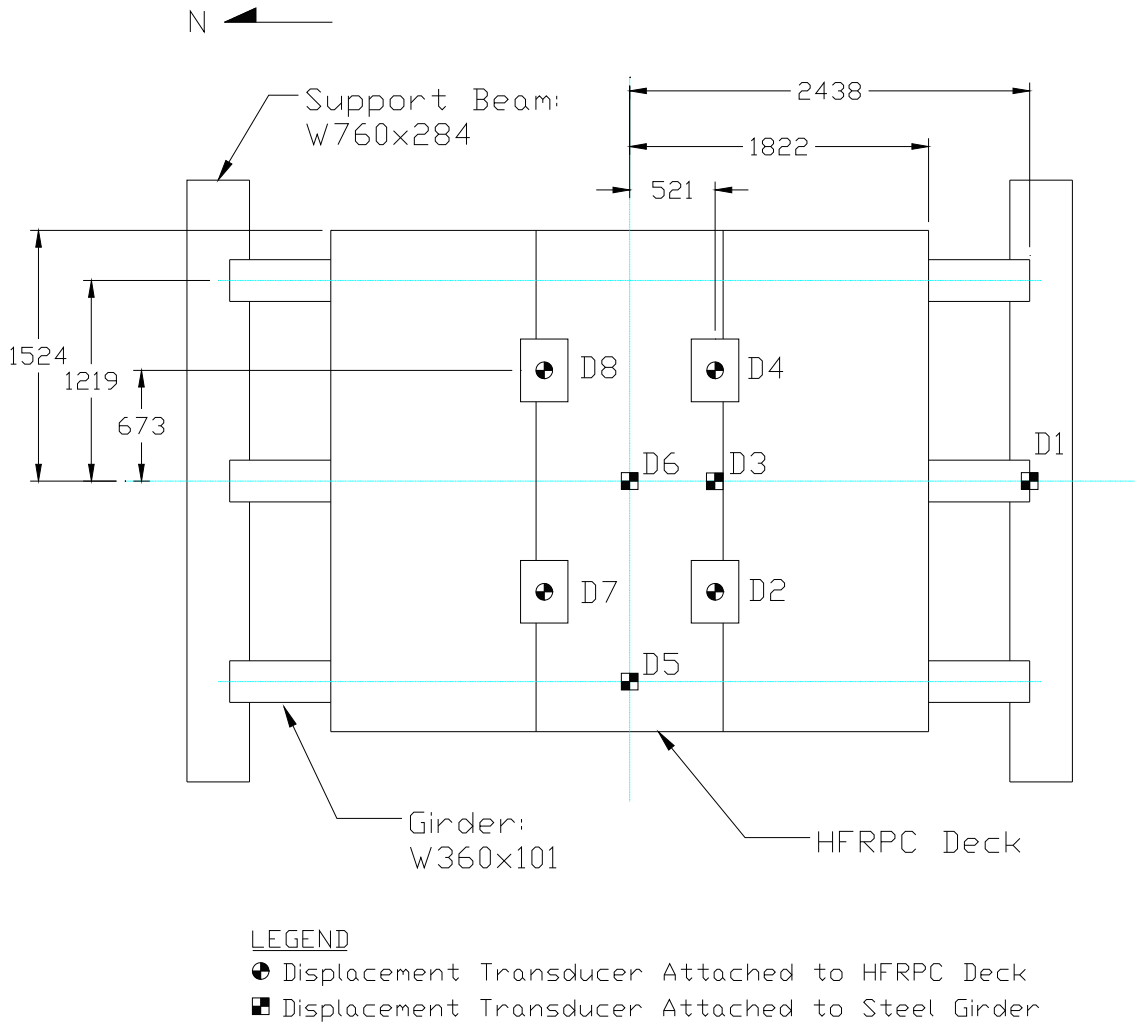

Fig. 3.2 Plan view of specimen showing instrumentation layout

3.4 Experimental Results

This section presents the results from creep testing performed on the HFRPC system. The primary results are the average daily vertical displacements that show the creep behavior of the HFRPC deck and HFRPC system. Additionally, the average daily temperature is reported for the duration of the test to illustrate the range and fluctuation of the surface temperature of the HFRPC deck.

Figure 3.3a presents the vertical displacement results for the HFRPC deck (denoted HFRPC) and the steel girders. In this figure average daily vertical displacement results are plotted against time where zero on the time axis represents the initial vertical displacement of the specimen after being loaded. Creep in the HFRPC deck is evident in Fig. 3.3a from the increase in vertical displacement observed at the points of loading (transducers D2, D4 and D8) up to day 51 (unloading). Transducer D7 malfunctioned during the creep test and therefore results from this transducer are not presented. Creep displacements in the HFRPC ranged from 15 (D2) to 20 (D4) percent of the initial vertical displacement. The vertical displacement of the steel girders (D3, D5 and D6) provide an idea of the creep behavior of the HFRPC system, that is the HFRPC deck and steel girders. The results presented in Fig. 3.3a show the vertical displacement of the steel girder (D5 and D6) remained relatively constant for the 51 day period while the specimen was loaded then rapidly decreased on day 51 when the specimen was unloaded. This result suggests the creep behavior of the HFRPC deck had a negligible effect on the global creep behavior of the specimen. Upon unloading the specimen, approximately 95 percent of the initial vertical displacement in the steel girders (D5 and D6) was recovered. In the HFRPC deck between 82 and 84 percent of the initial vertical displacement was recovered upon unloading representing the elastic recovery of the HFRPC system. The vertical displacement of the HFRPC continued to recover until the conclusion of the creep test at which time the vertical displacements in the HFRPC deck were approximately 0.5 mm.

Figure 3.3b present average daily temperature data for the duration of the creep test. From Fig. 3.3b the temperature of the top surface ranged from, approximately, 22 ^{o}C to 19 ^{o}C for the duration of the test and can be attributed to the change in the ambient

temperature of the testing laboratory over the 73 day test. The temperature of the bottom surface of the HFRPC deck ranged from 21 ^{o}C to 18 ^{o}C, a three degree change that again can be attributed to the change in ambient temperature of the testing laboratory. Also from, Fig. 3.3b the temperature value of the top and bottom thermocouples differs by approximately 1 ^{o}C throughout the duration of the test. This difference is due to error in the calibration of the thermocouple and does not represent a true physical difference. The results presented show that the HFRPC specimen was subjected to only a minor deviation in ambient temperature (approximately 3 ^{o}C) and that throughout the duration of the test the temperature of the specimen remained well below a temperature at which the mechanical properties of the GFRP (Glass Fiber Reinforce Polymer) would be affected.

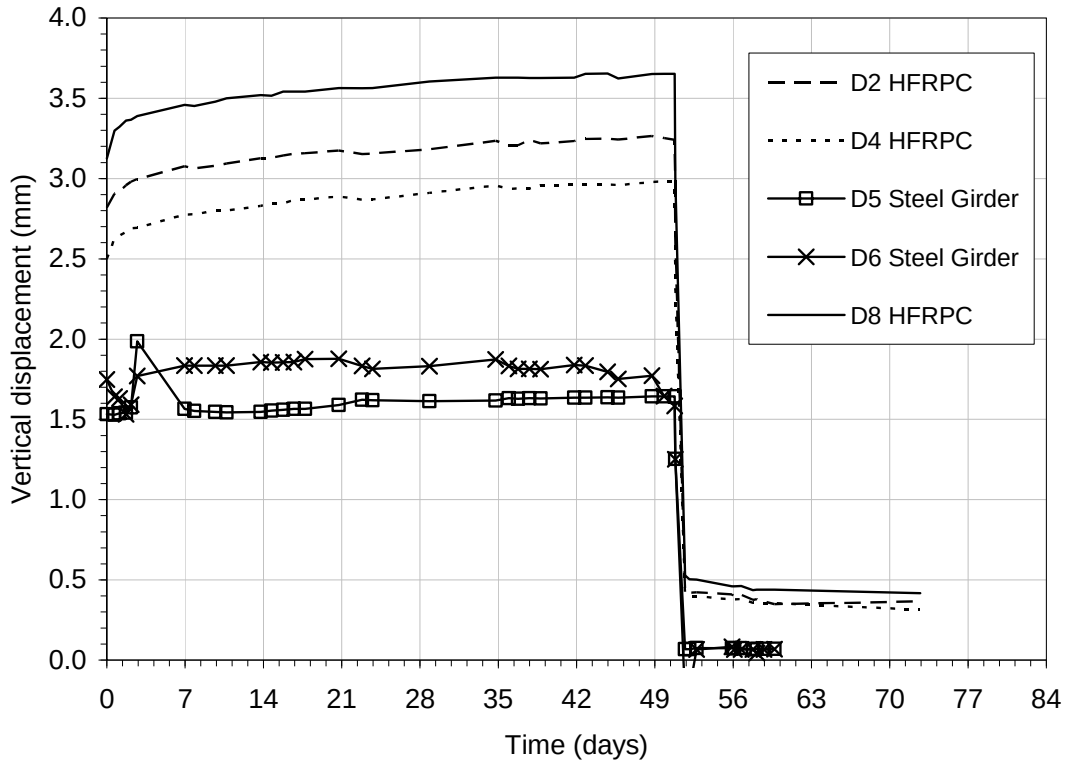

a. vertical displacement

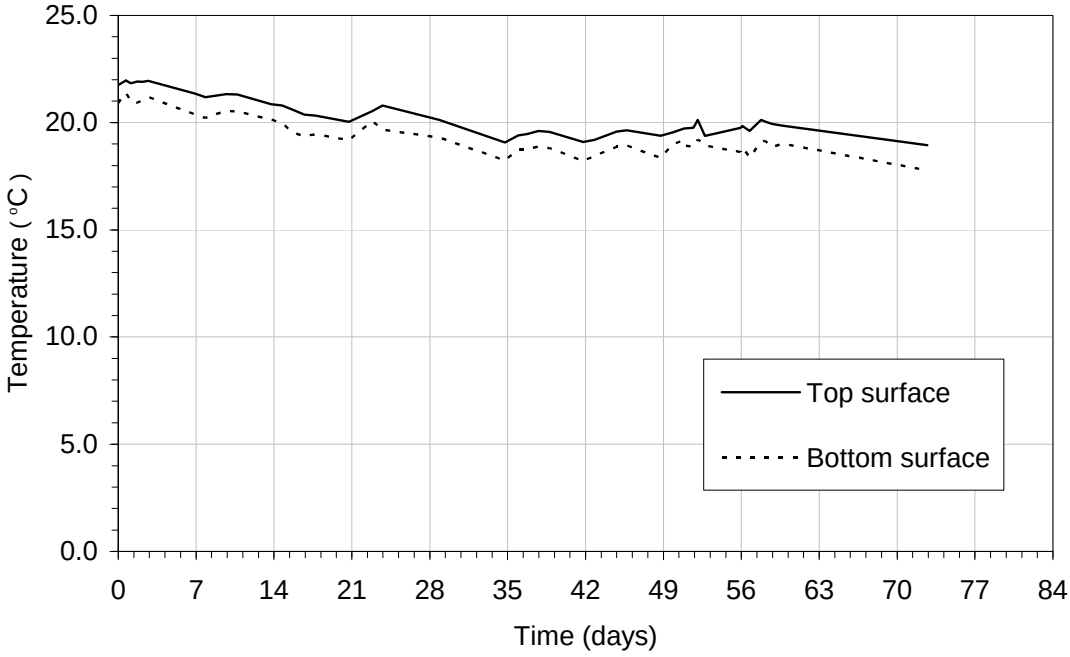

b. temperature

Fig. 3.3 Results of creep testing

SECTION 4

FATIGUE TESTING

4.1 General

Fatigue testing was performed to investigate the fatigue resistance of the HFRPC specimen to gain an improved understanding of the long term behavior of the hybrid bridge deck and steel girder system (HFRPC-SG). The fatigue testing program consisted of subjecting the HFRPC-SG specimen to 2 million cycles of dynamic loading with amplitude of approximately 1.33 times the scaled tandem load. Throughout the fatigue testing program, "benchmark" static tests were performed at 200,000 cycle intervals to monitor the stiffness of the HFRPC-SG specimen and composite behavior between the HFRPC bridge deck and steel girders. This section presents a summary of the experimental setup, the fatigue testing program and results from the benchmark 200,000 cycle static tests.

4.2 Experimental Setup

The experimental setup for the fatigue testing program was designed to enable subjecting the HFRPC-SG specimen to 2 million cycles of vertical loading with amplitude of 165 kN (1.33 times the scaled tandem load). A photograph showing the experimental setup for the fatigue testing program is presented in Fig. 4.1. Figures 4.2 and 4.3 present schematics of the experimental setup that consisted of the HFRPC–SG specimen (including HFRPC deck and steel girders) simply supported on two W760x284 transverse support beams, a spreader frame to simulate a two axle truck, four 383 mm by 290 mm steel plates with bonded rubber pads to simulate truck tires, a 500 kN (110 kip) MTS 244.41 hydraulic actuator and a vertical reaction frame consisting of two W310x60 columns and a W460x158 transverse beam. The vertical planar reaction frame is braced in the lateral direction (north-south) via two HSS steel sections connected to an existing steel reaction frame in the Structural Engineering and Earthquake Simulation Laboratory (SEESL) [see Fig. 4.2]. Load was applied via the hydraulic actuator to the HFRPC deck through the spreader frame and the four steel-rubber pads. The spreader frame and steel

pads were designed to simulate the dimensions and loading of the tandem load specified in the 1998 AASHTO LRFD Bridge Design Specifications (AASHTO 1998) scaled according to the 3/4 model length scale factor. Each steel-rubber pad consists of a steel plate 25 mm thick bonded to a rubber pad 12.5 mm thick each with plan dimensions of 383 mm by 290 mm and arranged in a two-axle truck configuration with 0.9 m between each axle (north-south) and a width of 1.35 m (east-west).

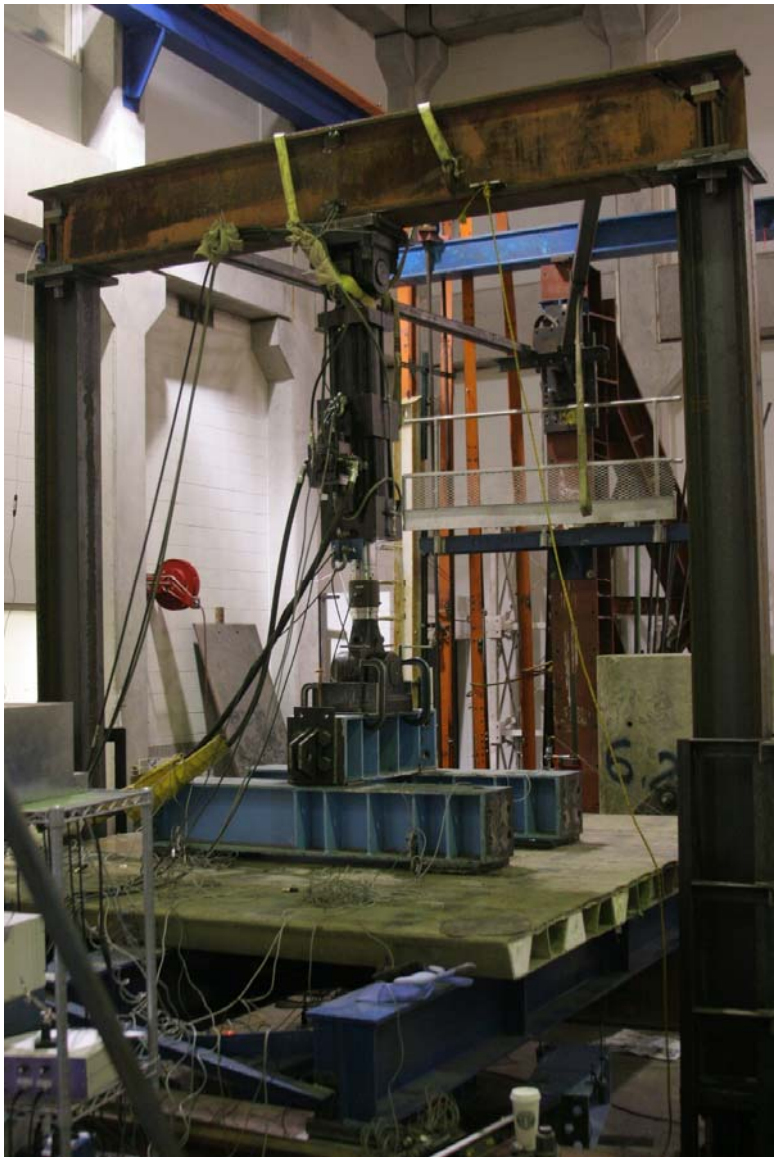

Fig. 4.1 Photograph of fatigue test setup

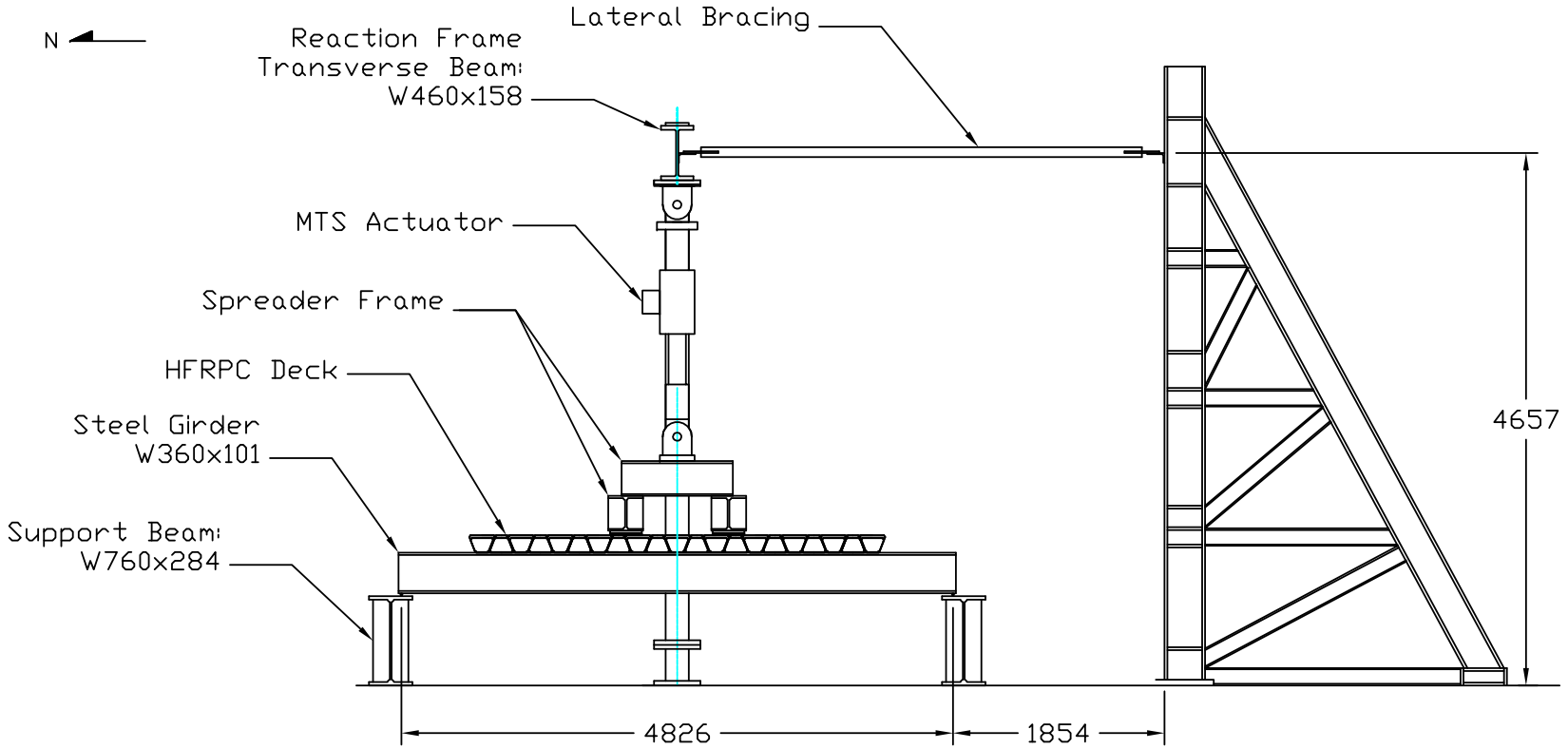

Fig. 4.2 Schematic showing side view of fatigue testing setup (dimensions in mm)

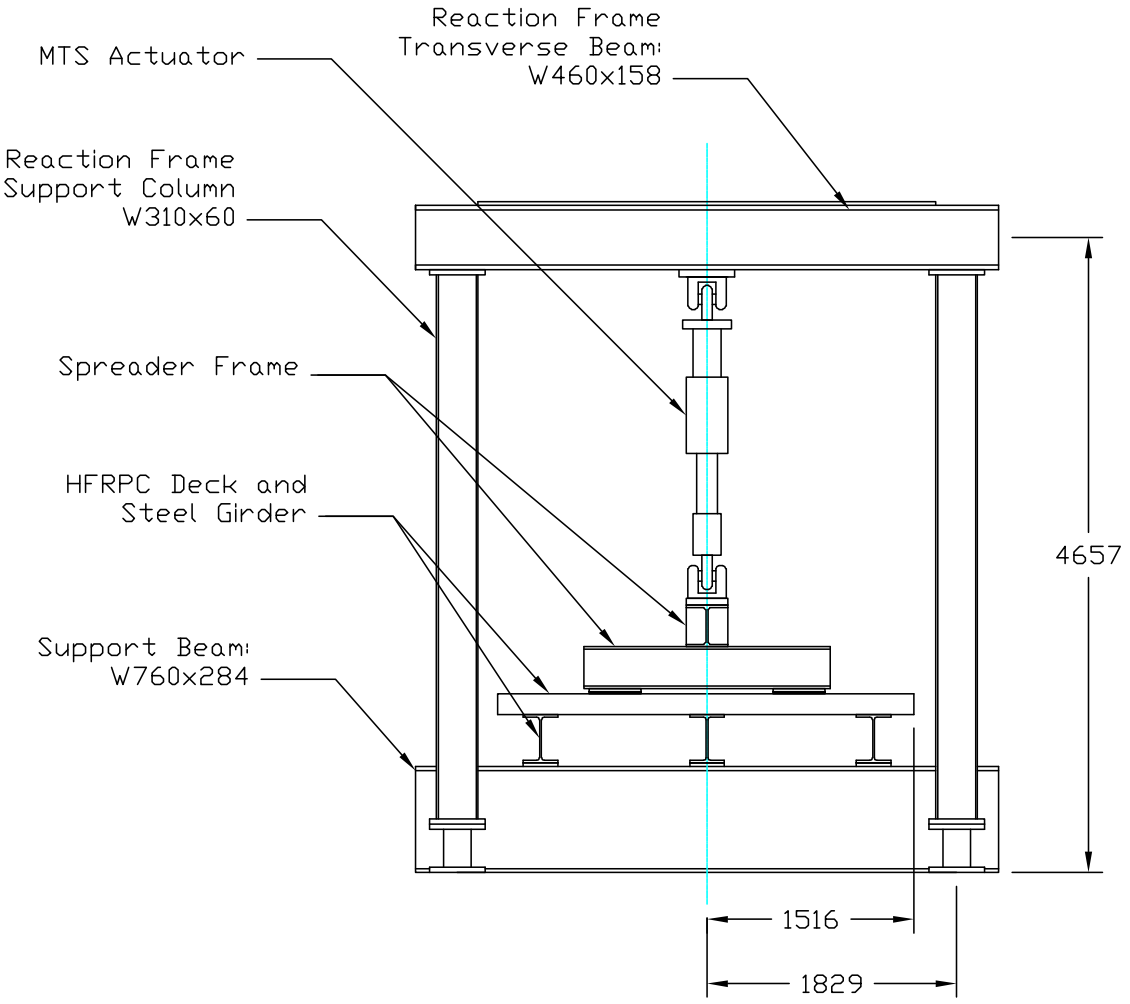

Fig. 4.3 Schematic showing elevation view of fatigue testing setup (dimensions in mm)

4.3 Instrumentation

4.3.1 General

Various instruments and a data acquisition system were used to measure and record the response of the HFRPC-SG specimen and the experimental setup throughout the fatigue testing program. Table 4.1 provides a list of instruments including identification (ID), type, range and description of location on the specimen. The instrumentation for the fatigue test consisted of: eight ±50 mm linear variable displacement transducers (LVDT); two ±540 mm string potentiometers (String Pot.); four ±25 mm linear potentiometers (Linear Pot.); eight uni-axial strain gages; three thermocouples; a uni-axial load cell in-line with the MTS actuator; and a ±127 mm LVDT housed in the MTS actuator. Figure

4.4 presents the instrumentation layout for the fatigue testing program shown on a plan view of the specimen including a legend and ID to identify the type and number of the instrument at a given location. Specifics pertaining to the type and placement of the instruments are discussed in the subsequent sections.

Table 4.1 List of Instruments

ID	Type	Range	Location
D1	LVDT	±50 mm	Top of center girder at south support
D2	LVDT	±50 mm	Bottom of HFRPC at south-west point of loading
D3	LVDT	±50 mm	Bottom of center girder at south line of loading
D4	LVDT	±50 mm	Bottom of HFRPC at south-east point of loading
D5	LVDT	±50 mm	Bottom of west girder at center of span
D6	LVDT	±50 mm	Bottom of center girder at center of span
D7	LVDT	±50 mm	Bottom of HFRPC at north-west point of loading
D8	LVDT	±50 mm	Bottom of HFRPC at north-east point of loading
D9	String Pot.	±540 mm	Top of east reaction frame support column
D10	String Pot.	±540 mm	Top of east reaction frame support column
D11	LVDT	±127 mm	LVDT housed in MTS actuator
D12	Linear Pot.	±25 mm	South-west steel-rubber pad
D13	Linear Pot.	±25 mm	South-east steel-rubber pad
D14	Linear Pot.	±25 mm	North-west steel-rubber pad
D15	Linear Pot.	±25 mm	North-east steel-rubber pad
S1	Strain Gage	±50000 μs	East girder top flange
S2	Strain Gage	±50000 μs	East girder web
S3	Strain Gage	±50000 μs	East girder web
S4	Strain Gage	±50000 μs	East girder bottom flange
S5	Strain Gage	±50000 μs	Center girder top flange
S6	Strain Gage	±50000 μs	Center girder web
S7	Strain Gage	±50000 μs	Center girder web
S8	Strain Gage	±50000 μs	Center girder bottom flange
F1	Load Cell	±448 kN	In-line with MTS Actuator
TH1	Thermocouple	-29 to 149 ^{o}C	Top HFRPC surface at south-east point of loading
TH2	Thermocouple	-29 to 149 ^{o}C	Bottom HFRPC surface at south-east point of loading
TH3	Thermocouple	-29 to 149 ^{o}C	Ambient

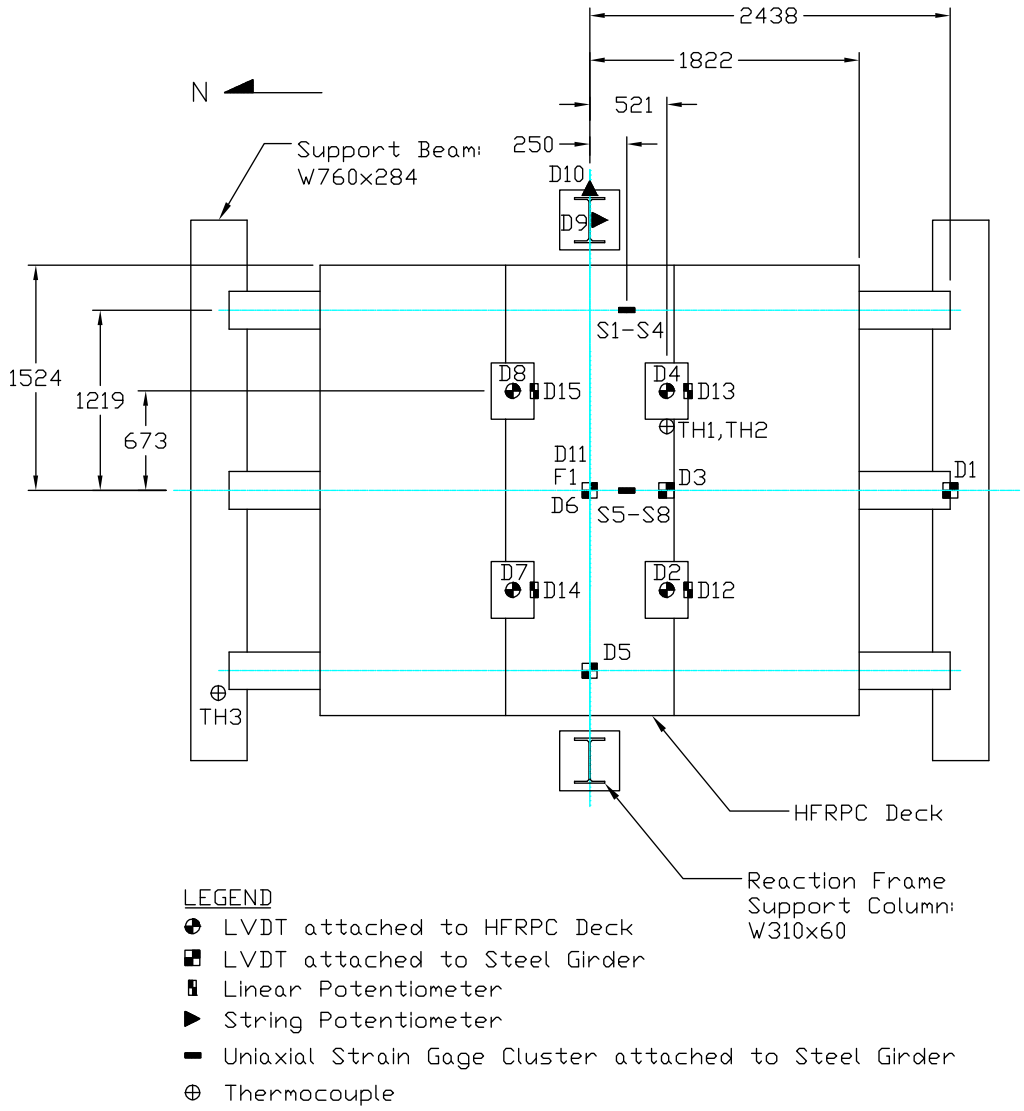

Fig. 4.4 Plan view of specimen showing instrumentation layout (dimensions in mm)

4.3.2 HFRPC-SG Specimen

The global behavior of the HFRPC-SG system was monitored using a combination of LVDTs and the actuator load cell. The vertical displacement of the steel girders were measured at the centerline (D5 and D6) and line of loading (D3) using LVDTs anchored to the strong floor and attached to the underside of the interior and west exterior girder. The vertical displacement at the south support was measured using a single LVDT (D1) the relative displacement of the bridge specimen could be calculated in the event of support displacements. The force applied to the bridge specimen was measured and

recorded via the in-line uni-axial actuator load cell (F1). The load cell data (F1) in conjunction with the LVDT data (specifically D6) were used to plot the global force-displacement response of the HFRPC-SG specimen to facilitate the calculation of the global vertical stiffness throughout the fatigue testing program. String potentiometers (D9 and D10) were mounted on a reference frame and attached to the transverse reaction frame used to monitor movement of the frame that might develop should the bolted connections loosen at any point during the fatigue test.

4.3.3 HFRPC Bridge Deck

The behavior of the HFRPC bridge deck was monitored using a combination of LVDTs, linear potentiometers, actuator load cell and three thermocouples. The vertical displacement of the HFRPC under each of the four loading points was measured and recorded using four LVDTs (D2, D4, D7 and D8). The vertical deformation of each of the four elastomeric pads was measured and recorded using four linear potentiometers (D12 – D15). As a precautionary measure, three thermocouples were installed on the specimen to measure the ambient (TH3) temperature and the temperature of the bride deck surface (TH1 and TH2) due to the thermal sensitivity of the GFRP material and the frequency and duration of the fatigue loading. Thermocouples TH1 and TH2 were mounted adjacent to the south-east point of loading with TH1 and TH2 on the top and bottom surfaces of the HFRPC deck, respectively.

4.3.4 Composite Behavior

Strain gages installed at two locations were used to measure and record longitudinal strain at various heights on the steel girders so that strain profiles could be used to determine and monitor the location of the neutral axis – an indicator of composite action between the HFRPC bridge deck and supporting steel girders. Two clusters of four uni-axial gages were installed approximately 250 mm from the centerline of the interior (S5-S8) and east exterior girder (S1-S4) as illustrated in Fig. 4.4. The uni-axial strain gages were installed at various heights on the steel girders and oriented to measure longitudinal strain. Figure 4.5 presents a cross-sectional view of a steel girder illustrating the location of the individual strain gages on the girder cross-section.

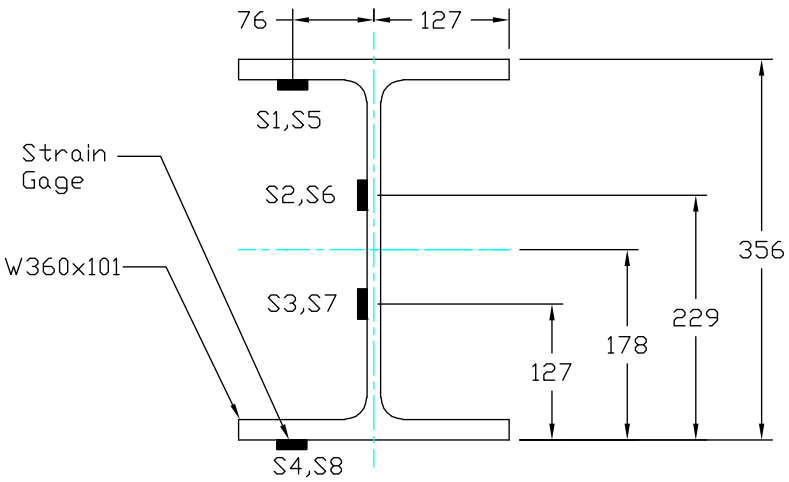

Fig. 4.5 Uniaxial strain gage cluster attached to steel girder (dimensions in mm)

4.4 Experimental Protocol

The experimental protocol was designed to investigate the fatigue resistance of the HFRPC bridge deck and composite steel girder system. The fatigue test consists of 2 million cycles of constant amplitude load applied dynamically to the HFRPC specimen with static tests performed at 200,000 cycle intervals throughout the duration of the fatigue test to monitor changes in the stiffness or composite behavior of the HFRPC-SG specimen. Due to safety and operational concerns the fatigue test could not be conducted continuously (without interruption). Instead the specimen was subjected to 2 million cycles over a 35 day period with daily testing durations ranging from approximately 3-1/2 hours to 13 hours of continuous testing. Cycles of loading were tracked (counted) based on the daily duration of constant amplitude loading and the loading frequency of 2 Hz.

Load was applied via the servo-hydraulic actuator using force control and a sinusoidal wave form in three phases: Ramp-up, Constant amplitude and Ramp-down. The three-phase loading scheme was utilized to ensure stability of the hydraulic actuator using force control at the target frequency of 2 Hz. An illustration of the three-phase loading scheme is presented in Fig. 4.6a. The Ramp-up phase consisted of 54 cycles of sinusoidal loading with increasing amplitude up to 156 kN (1.26 x Tandem Load) with a duration of 27 seconds. Figure 4.6b presents a portion of the Ramp-up phase to illustrate the frequency and sinusoidal wave form of the loading. The constant amplitude (testing) phase

consisted of sinusoidal loading with amplitude of 156 kN for the daily duration of testing (ranging from 3-1/2 hours to 13 hours). The Ramp-down phase consisted of 54 cycles of decreasing amplitude sinusoidal cycles until the structure was effectively un-loaded. For the purpose of cycle counting the Ramp-up and Ramp-down phases were ignored using only the Constant amplitude duration and the 2 Hz frequency to determine the daily number of cycles conducted. At intervals of 200,000 cycles, a static test was performed to collect data and to determine the stiffness and composite behavior of the HFRPC-SG systems. Each static test consisted of loading the HFRPC-SG specimen from a preload of approximately 9 kN up to 156 kN (1.26 x Tandem Load) and back to the 9 kN preload. Results of the static tests were used to investigate the fatigue resistance of the HFRPC-SG specimen and are presented in the subsequent results section.

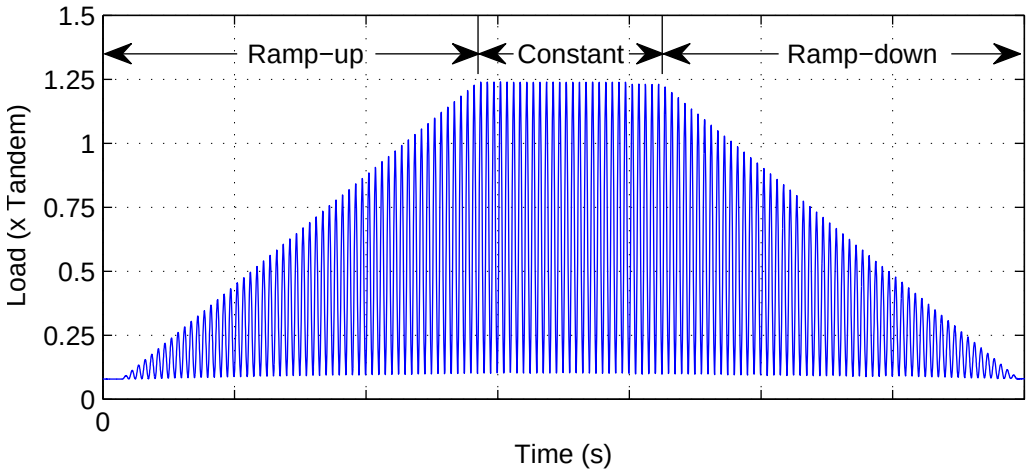

a. Three-phase loading scheme

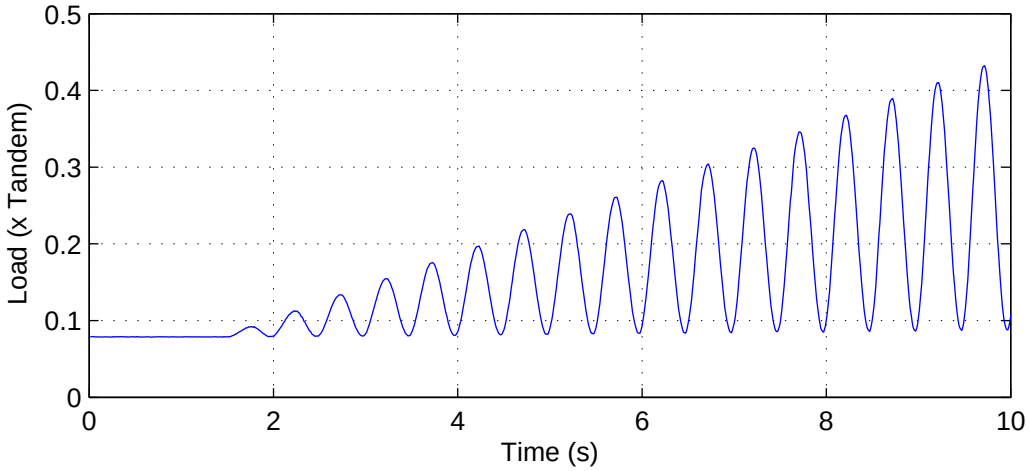

b. Portion of the Ramp-up phase

Fig. 4.6 Three phase loading scheme used for fatigue testing

4.5 Experimental Results

4.5.1 General

The results of the static "benchmark" tests performed at intervals of 200,000 cycles were used to determine: the global stiffness of the HFRPC-SG system; the local stiffness of the HFRPC bridge deck; and the location of the neutral axis of bending at one location on each of the interior and east exterior girders. These quantities were tracked throughout the duration of the fatigue test to identify potential change (degradation) of the HFRPC bridge deck and composite HFRPC-SG system and ultimately used to determine the fatigue resistance of the HFRPC-SG specimen.

The subsequent sections provide detailed descriptions for the determination of the stiffness and neutral axis quantities including sample results for the global, local and composite behavior of the HFRPC-SG system. The fatigue test concluded with an estimated 2,000,092 cycles after 35 nonconsecutive days of testing. Figure 4.7 presents a cumulative cycle history for the fatigue test with an average of 57,145 cycles per day at a 2 Hz frequency or approximately 8 hours of testing per day.

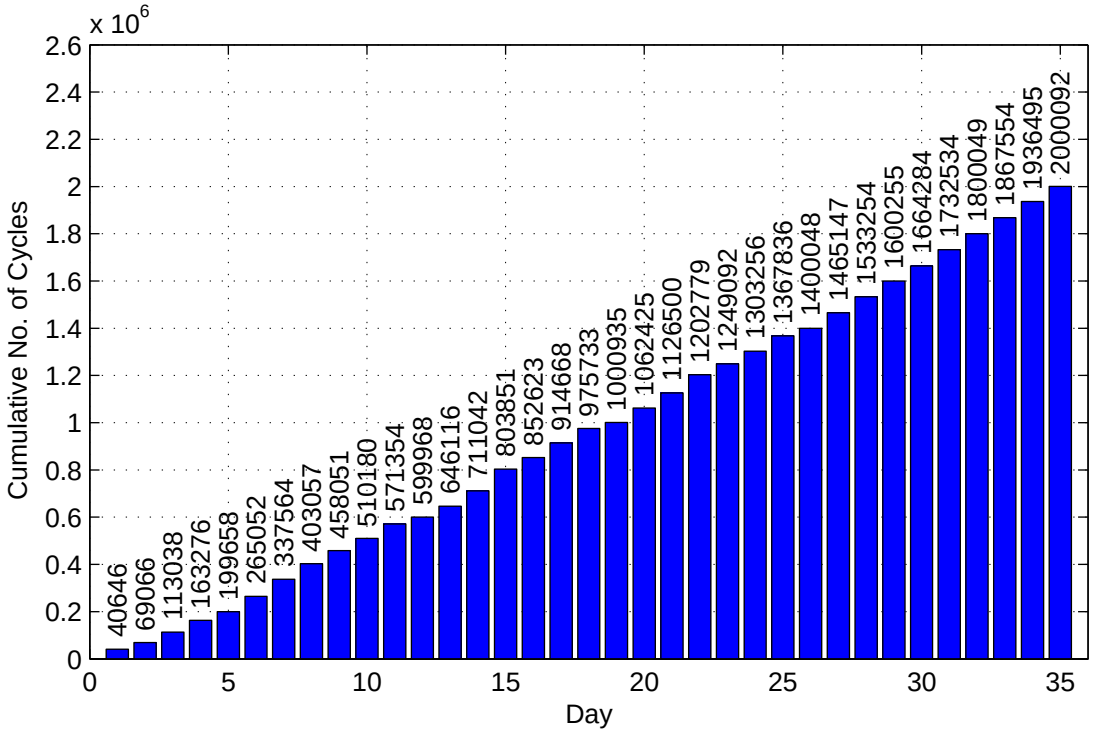

Fig. 4.7 Loading history of fatigue test

The peak load amplitude for the fatigue testing was decreased from the target value of 1.33 times the scaled tandem load (165 kN) to approximately 1.26 times the scaled tandem load (156 kN) to ensure the 2 Hz loading frequency could be maintained by the hydraulic actuator in a stable manner throughout the duration of testing. For consistency the static "benchmark" tests were also conducted to a peak load amplitude of 1.26 times the scaled tandem load or 156 kN. Although the load amplitude of 1.26 times the scaled tandem load is less than the desired 1.33 times the scaled tandem load that was chosen to account for the AASHTO impact factor the achieved load level of 156 kN is significantly (26 percent) larger than the scaled tandem load of 124 kN.

4.5.2 HFRPC-SG Specimen

The vertical displacement at the center of interior girder (D6) and the applied load (F1) data were used to determine the force-displacement response of the global HFRPC-SG system at specific intervals throughout the fatigue test and to calculate the stiffness of the global system. Sample force-displacement results from static benchmark tests performed at approximate 400,000 cycle increments are presented in Fig. 4.8 including the initial (0 cycles) static benchmark test (Fig. 4.8a). From the results presented in Fig. 4.8, the force-displacement response of the HFRPC-SG bridge system is nearly linear for all benchmark tests with a consistent displacement response of approximately 1.9 mm at 150 kN of applied load. The results presented in Fig. 4.8 suggest the stiffness of the HFRPC-SG bridge system did not degrade through the duration of the fatigue test given the similarity of the initial (Fig. 4.8a) force-displacement response and the response after approximately 2 million cycles (Fig. 4.8f).

To further verify that the global stiffness remained constant and that degradation of the HFRPC-SG was not observed after 2 million cycles, the global vertical stiffness of the HFRPC-SG was calculated from the static benchmark data (D6 and F1) for each 200,000 cycle interval. From each 200,000 cycle static benchmark test the vertical stiffness of the HFRPC-S G system was calculated using linear regression analysis of the data on the ascending branch of the load curve between 0.2 and 0.8 times the maximum load (approximately 156 kN).

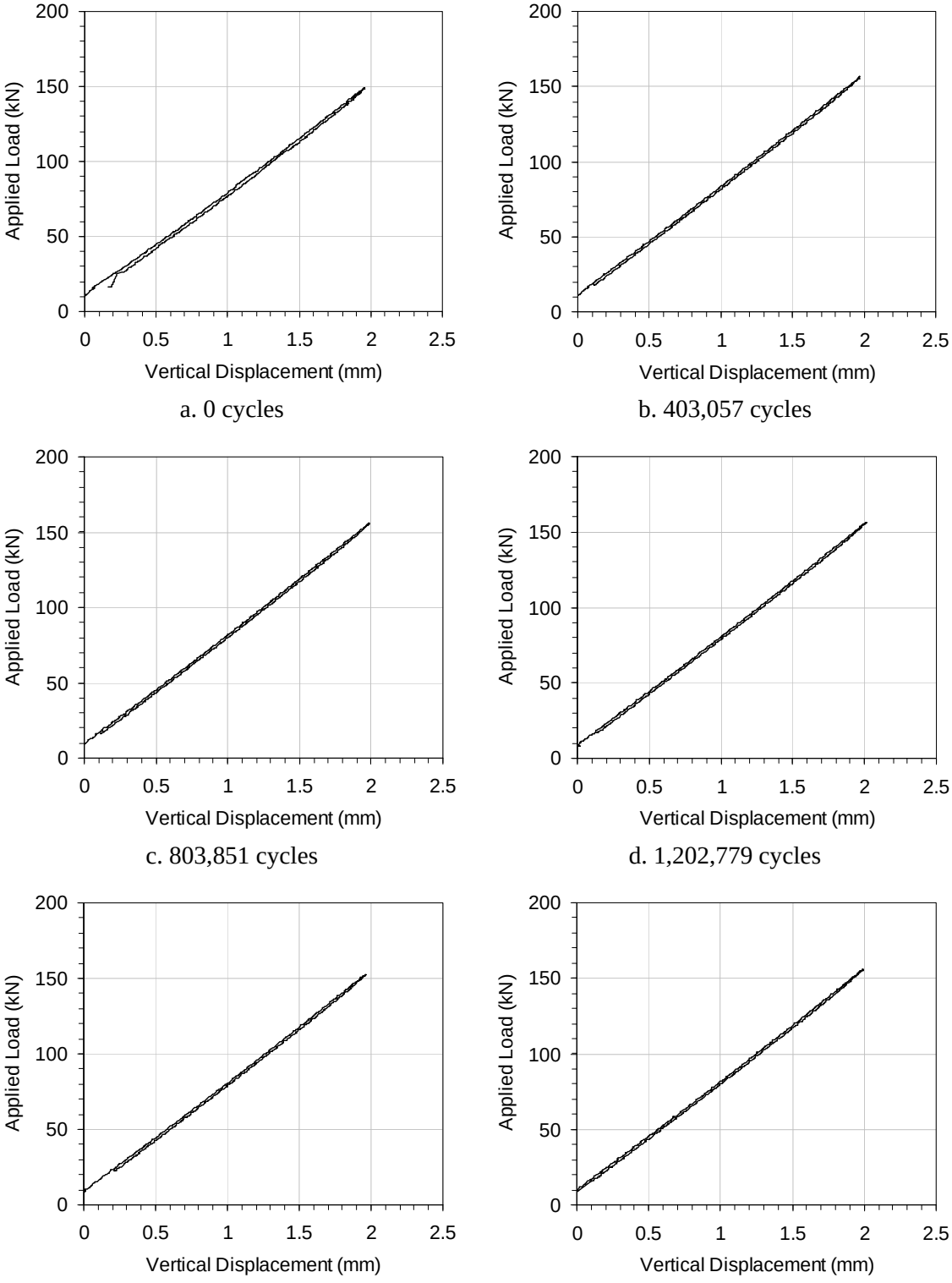

a. 0 cycles

b. 403,057 cycles

c. 803,851 cycles

d. 1,202,779 cycles

e. 1,600,255 cycles

f. 2,000,092 cycles

Fig. 4.8 Global HFRPC-SG force-displacement results from various static test performed throughout the fatigue testing program

The results of the vertical stiffness calculation for each of the eleven static benchmark tests performed throughout the fatigue test are plotted in Fig. 4.9.a. The initial (0 cycles) vertical stiffness of the HFRPC-SG system was determined to be 73 kN/mm. Figure 4.9b presents vertical stiffness results for each benchmark test normalized by the initial vertical stiffness (73 kN/mm). The normalized results provide an indication of the percent change in vertical stiffness over the course of the fatigue test. From Fig. 4.9b an approximate 3 percent increase in stiffness is observed from 0 cycles to 200,000 cycles then remains relatively constant between 1.03 and 1.04 through to 2 million cycles. The 3 percent increase observed between 0 and 200,000 cycles is likely due to the replacement of the D6 LVDT displacement transducer that malfunctioned sometime between these two static benchmark tests. If the initial value is neglected the change in stiffness for the remaining 1.8 million cycles was observed to be less than 1 percent.

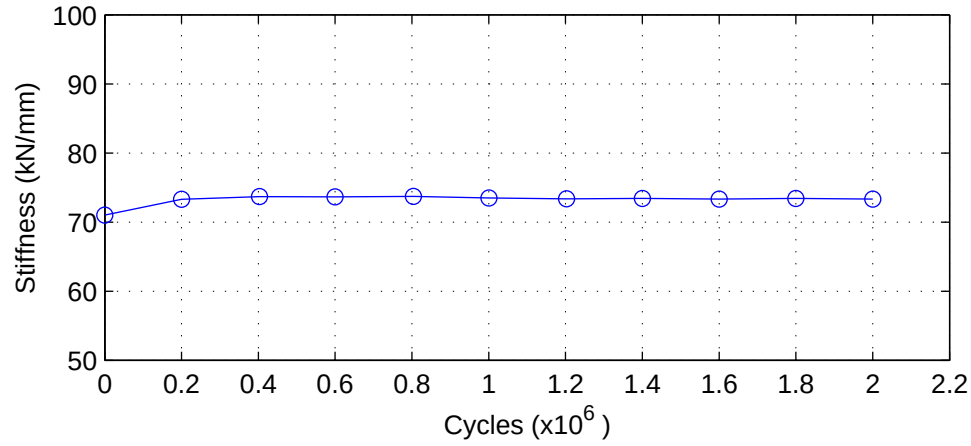

a. vertical stiffness

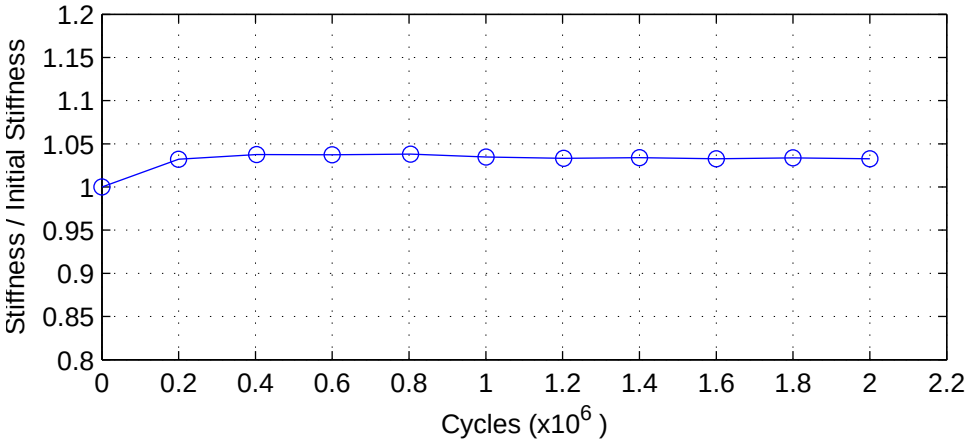

b. normalized vertical stiffness

Fig. 4.9 Vertical stiffness results for the HFRPC-SG specimen

4.5.3 HFRPC Bridge Deck

Vertical displacement data for the HFRPC deck at each point of loading (D2, D4, D7 and D8) were utilized with the applied load (F1) to calculate the local stiffness of the HFRPC deck for each static benchmark test. Using the calculated local stiffness the fatigue resistance of the HFRPC deck was monitored throughout the duration of the 2 million cycles of loading. However, the absence of load cells at each load point (D2, D4, D7 and D8) required the load applied at each point to be determined indirectly using some of the displacement data and the actuator load cell data. Due to eccentricity in the load applied by the actuator and variations in the levelness of the bridge deck surface, the load transmitted to each point is unlikely to be equally distributed as suggested by the displacement data presented in Fig. 4.10a where the displacement recorded by D8 is approximately half that of D2 and D4.

The percent of the total applied load (F1) transmitted to each of the four loading points was estimated using equilibrium and the peak displacement data from the 2 million cycle static test (Fig. 4.10a) assuming the stiffness of the HFRPC bridge deck at each point of loading is equal – a reasonable assumption given the symmetry of loading and the manufacturing tolerances of the GFRP deck shell. Displacement data from the 2 million cycle static test was used in lieu of the 0 cycle static (initial) test data because the D2 displacement transducer did not measure during the initial test. From equilibrium:

$$P = F_{D2} + F_{D4} + F_{D7} + F_{D8} \tag{4-1}$$

where P is the applied load from the hydraulic actuator and F_{D2}, F_{D4}, F_{D7} and F_{D8} are the forces transmitted to the load points corresponding to the location of the D2, D4, D7 and D8 displacement transducers, respectively. Additionally the force at each load point has to be equal to the local stiffness (generalized vertical stiffness) of the HFRPC deck times the vertical displacement as follows:

$$F_{D2} = K_{D2} u_{D2} \tag{4-2}$$

where K_{D2} is the generalized stiffness of the HFRPC deck at the south-west point of loading. Similarly, the forces at the remaining points of loading can be expressed as:

$$F_{D4} = K_{D4} u_{D4} \tag{4-3}$$

$$F_{D7} = K_{D7} u_{D7} \tag{4-4}$$

$$F_{D8} = K_{D8} u_{D8} \tag{4-5}$$

Further assuming $K_{D2} = K_{D4} = K_{D7} = K_{D8} = K$ and substituting Eqs. 4-2, 4-3, 4-4 and 4-5 into Eq. 4-1 yields:

$$P = K \cdot \left(u_{D2} + u_{D4} + u_{D7} + u_{D8} \right) \tag{4-6}$$

From Eq. 4-6 the portion of the total load transmitted to a particular loading point is simply the ratio of the displacement at that location to the sum of all the vertical displacements, for example:

$$\frac{F_{D2}}{P} = \frac{u_{D2}}{\left(u_{D2} + u_{D4} + u_{D7} + u_{D8} \right)} \tag{4-7}$$

Using Eq. 4-7 and the vertical displacement data from the 2 million cycle static test the proportion of load transmitted to each of the four loading points were determined to be: $F_{D2} / P = 0.28$, $F_{D4} / P = 0.27$, $F_{D7} / P = 0.3$ and $F_{D8} / P = 0.15$. These ratios were then used to determine the proportion of total load transmitted to each load point and to facilitate the calculation of the local HFRPC bridge deck stiffness. The force-displacement response of the HFRPC bridge deck at each point of loading from the 2 million cycle static test are presented in Fig. 4.10b – 4.10e. Although not presented in this report an analysis of a simple four spring idealization of the HFRPC bridge deck with the displacement data suggested that eccentricities of the applied loading as small as 3 mm in the north-south direction and 0.1 mm in the east-west direction could have produced the observed difference in load transmitted to each loading point and resulting vertical displacement.

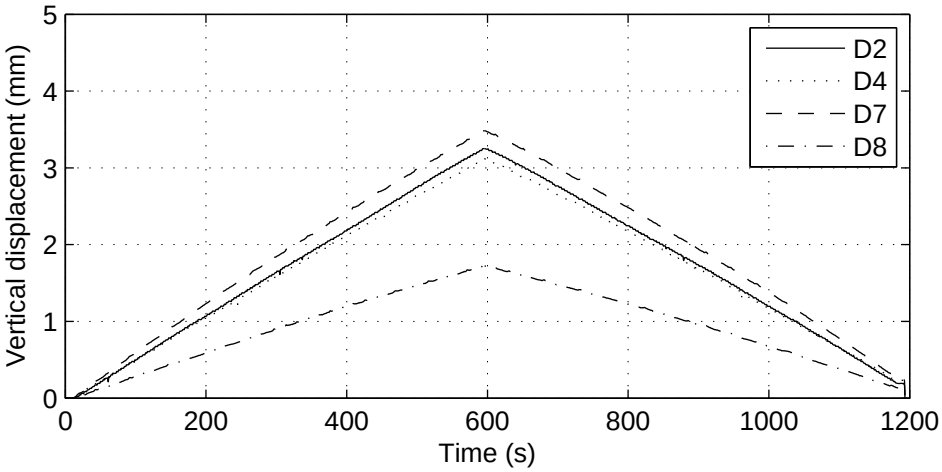

a. vertical displacement

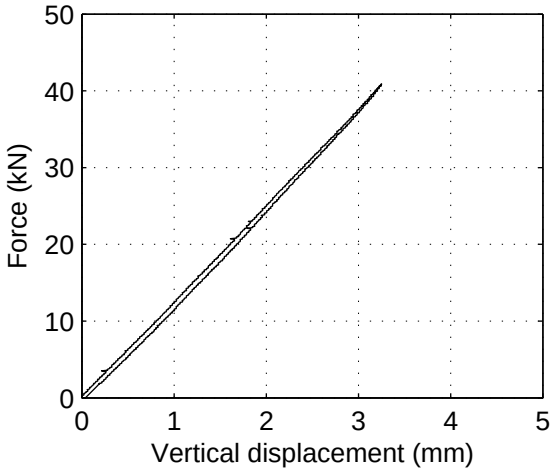

b. D2

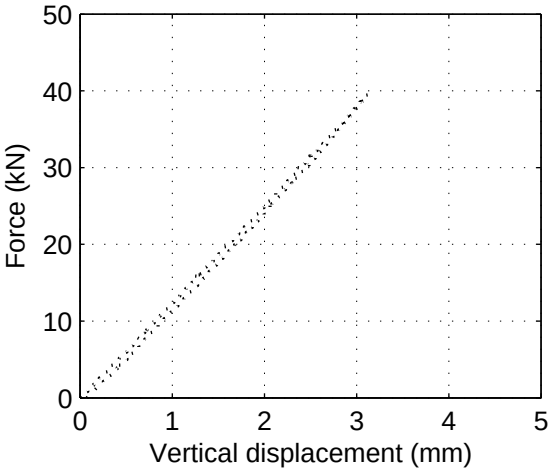

c. D4

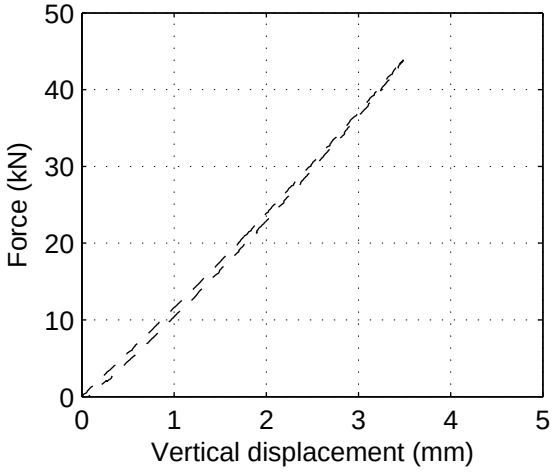

d. D7

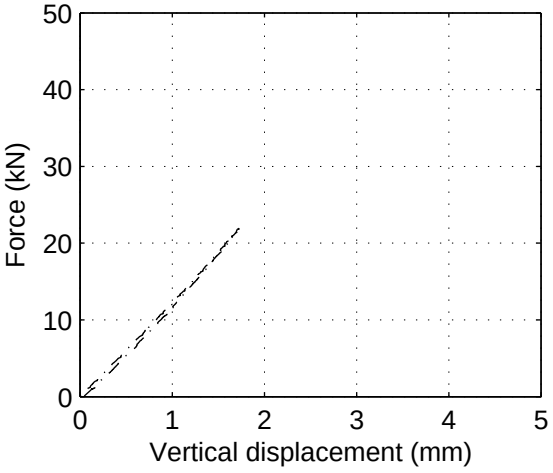

e. D8

Fig. 4.10 Vertical displacement and force-displacement response of HFRPC deck after 2,000,092 cycles

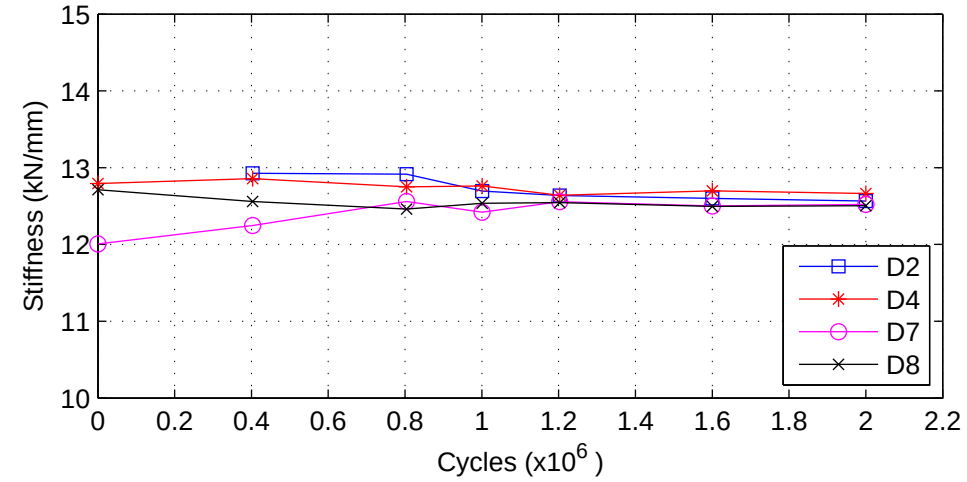

a. vertical stiffness

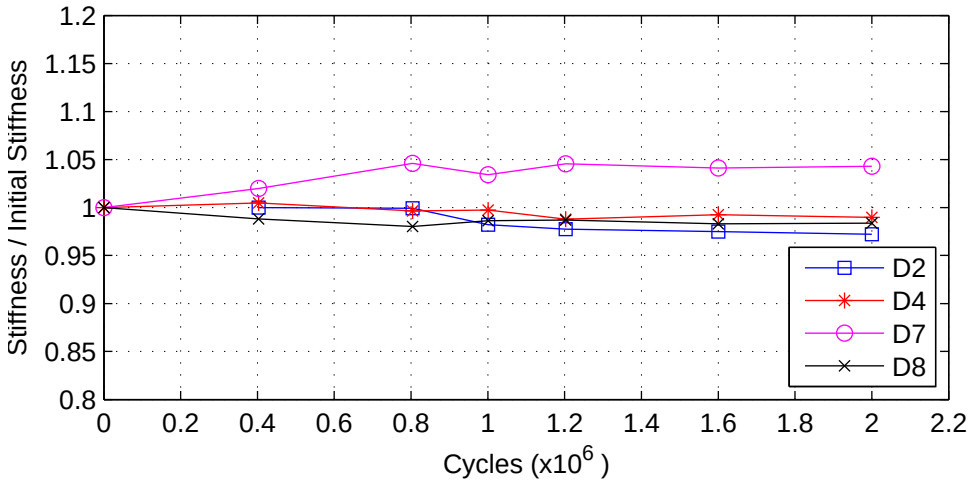

b. normalized vertical stiffness

Fig. 4.11 Vertical stiffness results for the HFRPC bridge deck

The load ratios derived previously from the 2 million cycle static test were used to determine the force-displacement response of the HFRPC bridge deck at each loading point for all the remaining static tests to facilitate the calculation of the local HFRPC deck stiffness. Similar to the calculation of the HFRPC-SG system stiffness (see Section 4.5.2), the local stiffness of the HFRPC bridge deck was calculated using linear regression analysis of the data on the ascending branch of the load curve between 0.2 and 0.8 times the maximum load at each load point (ranging from 23 kN to 46.5kN). Fig. 4.11 presents the local vertical stiffness of the HFRPC bridge deck calculated for each of the four points of loading (D2, D4, D7 and D8) for various static benchmark test from the initial (0 cycle) to the final after 2 million cycles. From the results presented in Fig. 4.11a the local stiffness ranged from approximately 12 kN/mm to 13 kN/mm. Figure 4.11b

presents the local vertical stiffness data normalized by the initial vertical stiffness noting no data was collected from D2 for the initial static test therefore the initial stiffness for D2 was taken from the 200,000 cycle static test. From the results presented in Fig. 4.11b, the total change in local stiffness at each location was less than 5 percent for the duration of fatigue test. Although the local stiffness at D2, D4 and D8 show a downward trend from the 0 cycle static test to the 2 million cycle static test the total change in the stiffness value is less than 3 percent.

4.5.4 Composite Behavior

The composite action between the HFRPC deck and steel girders was monitored using the position of the bending neutral axis at two locations. The neutral axis location was determined using longitudinal strain data from the strain gage sets installed on the interior (S5-S8, see Fig. 4.4) and exterior (S1-S4) girders collected for each static benchmark test. Figure 4.12 presents strain profiles at the exterior and interior girder locations for load levels of 0.4, 0.8 and 1.2 times the scaled tandem load for three different static tests: 0 cycles, 800,000 cycles and 2 million cycles. Each plot in Fig. 4.12 presents the longitudinal strain, in units of micro-strain (μ), plotted at four different heights of the (W360x101) girder section plotted as the height of the gage normalized by the depth of the section ($d = 356$mm). With the exception of the strain data from the exterior girder at 0 cycles (Fig. 4.12b) the strain profiles are nearly linear passing through zero strain at a normalized height of approximately 0.57 – representing the position of the neutral axis. A problem arose with the data acquisition system during the 0 cycle static test and the strain data for the exterior girders (S1-S4) was compromised hence the peculiar shape of the strain profiles presented in Fig. 4.12b.

The location of the neutral axis was calculated by linearly interpolating the strain data for all eleven static benchmark tests at each of the three load levels and was observed to range from $0.55d$ to $0.58d$ for all profiles. The approximate normalized neutral axis location of $0.57d$ being greater than half the section depth indicates the presence of composite action between the HFRPC deck and steel girders and the consistency of the location of the neutral axis ($0.55d$ to $0.58d$) at both locations throughout the fatigue test indicates the shear stud connection sufficiently resisted fatigue induced degradation.

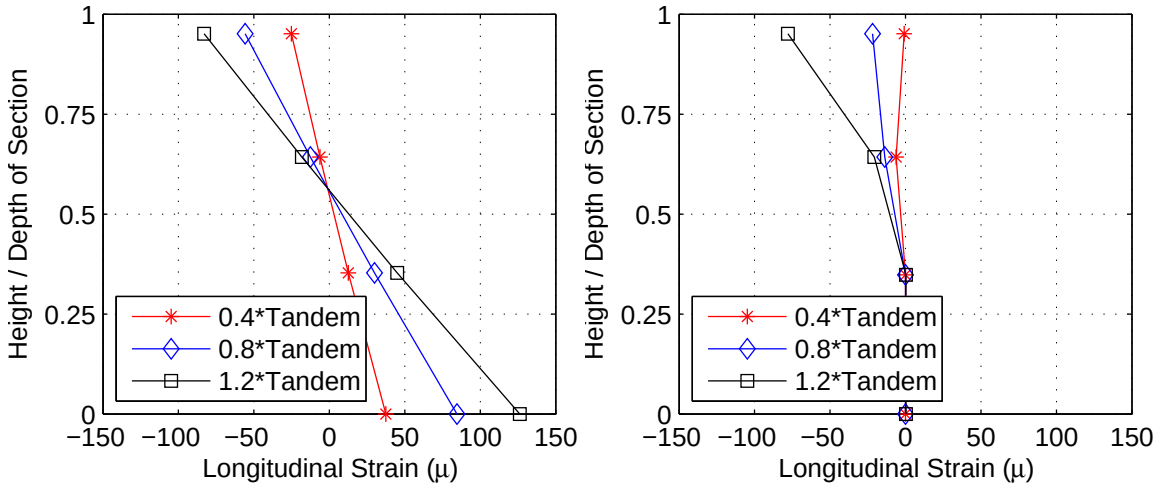

a. Interior Girder 0 cycles

b. Exterior Girder 0 cycles

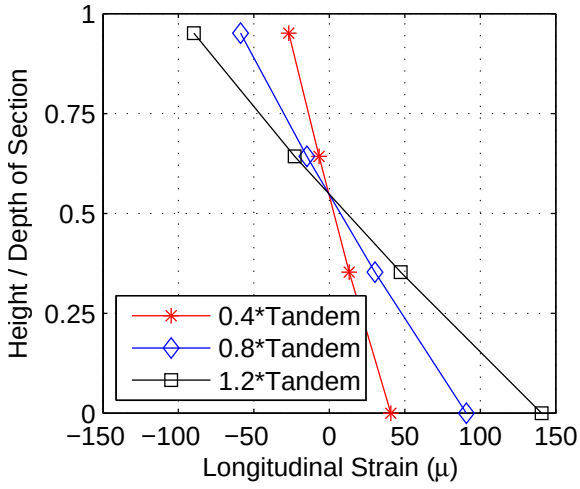

Interior Girder 803,851 cycles

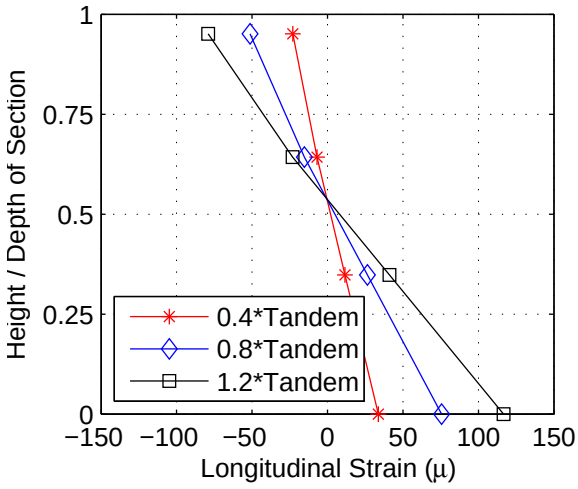

d. Exterior Girder 803,851 cycles

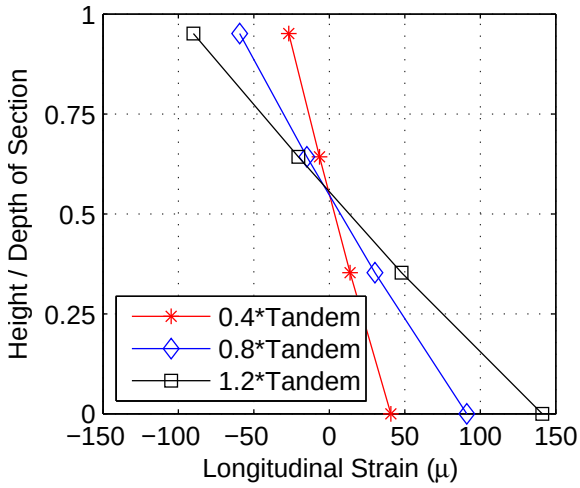

e. Interior Girder 2,000,092 cycles

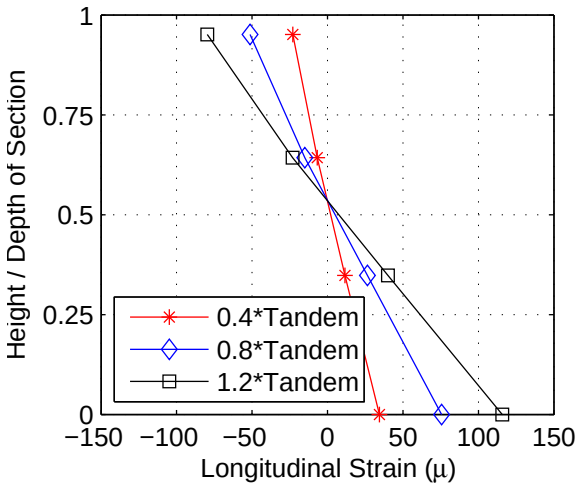

f. Exterior Girder 2,000,092 cycles

Fig. 4.12 Strain profiles across girders from various static benchmark tests

SECTION 5

ULTIMATE STRENGTH TESTING

5.1 General

Destructive testing was performed to investigate the ultimate capacity of the Hybrid Fiber Reinforced Concrete (HFPRC) bridge deck. Given the strength of the steel girders and the positioning of the four-point loading (centered between girders) it is unlikely that the capacity of the global HFRPC-SG system will be reached prior to exceeding the capacity of the HFRPC deck. The destructive test consists of subjecting the HFRPC-SG system to monotonically increasing vertical displacement until the first limit state (failure mode) has been reached (e.g., punching shear, loss of composite action, etc). Following observation of the first limit state the specimen will continue to be loaded with the goal of observing a second failure mode. Load will continue to be increased until it is judged no longer safe to continue with the test. Destructive testing will be conducted utilizing an experimental setup that was developed and used for previous service level verification tests performed on the HFRPC-SG system (Alnahhal 2007).

The following sections present summaries of the experimental setup, instrumentation, data reduction and results from destructive testing of the HFRPC-SG specimen.

5.2 Experimental Setup

The fatigue testing experimental setup (see Section 4) was designed specifically for the fatigue testing protocol (high frequency low amplitude loading) and therefore does not have sufficient capacity to reach the anticipated load level required to fail the HFRPC deck. To facilitate destructive testing of the HFRPC bridge deck an experimental setup with sufficient capacity used in previous verification tests performed on the HFRPC-SG specimen was utilized. A photograph of the experimental setup is presented in Fig. 5.1 showing the HFRPC-SG specimen, the loading frame, spreader frame and the two hydraulic actuators used to load the specimen.

Fig. 5.1 Photograph of destructive test setup

Schematics of the side and elevation view of the destructive testing setup are presented in Fig. 5.2. Again, the HFRPC-SG specimen was simply supported on two W760x284 support beams tied to the SEESL strong floor providing a span length of 4826 mm. Two Miller servo-hydraulic actuators each with 1110 kN of force capacity and ±203 mm of displacement capacity were connected to the strong floor and the loading frame via steel pedestal fixtures and hardware. In this configuration, contraction of the actuators would apply downward vertical loading to the HFRPC-SG specimen. The loading frame consists of a transverse (W460x158) beam with various web stiffeners and flange double plates attached to four stack beams each with web stiffeners at various locations. Similar to the fatigue testing setup, load is applied to the HFRPC-SG specimen at four points via a steel spreader frame and four 383 mm by 290 mm steel-rubber pads to simulate a two axle truck and the load applied by a truck tire. However for destructive testing the steel-rubber pads were rotated 90 degrees so that the 383 mm dimension was aligned with the north-south direction. This was done so that the edge of the pad did not coincide with the location of minor damage of the HFRPC deck that occurred during setup and is reflected in the instrumentation layout presented in the subsequent section.

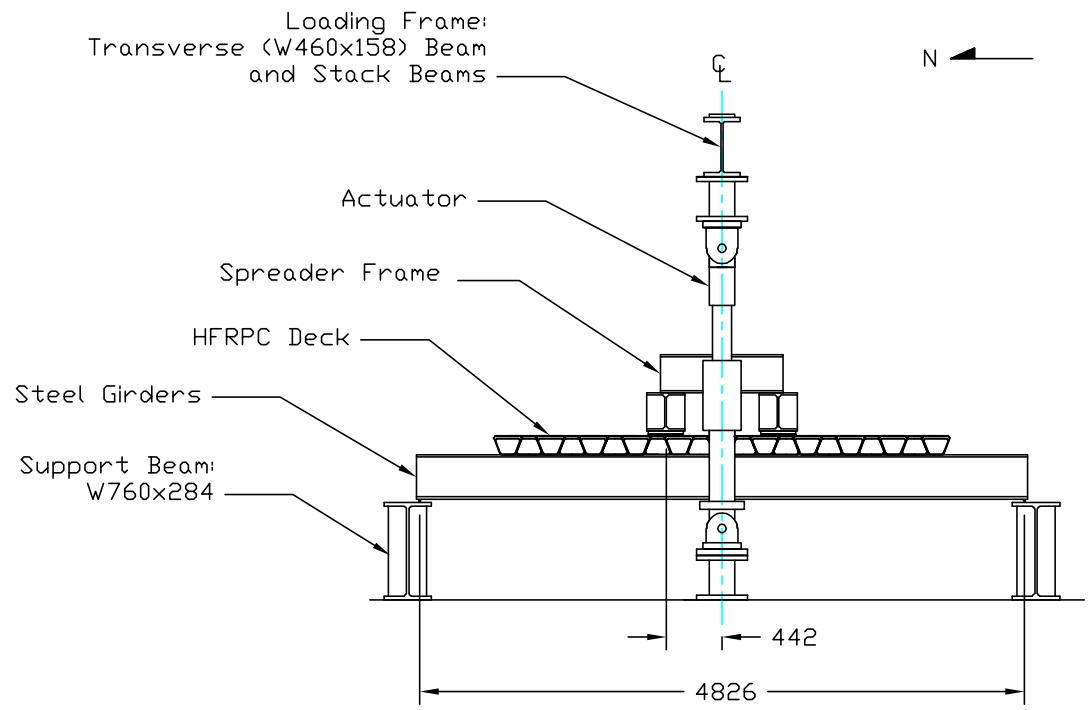

a. side

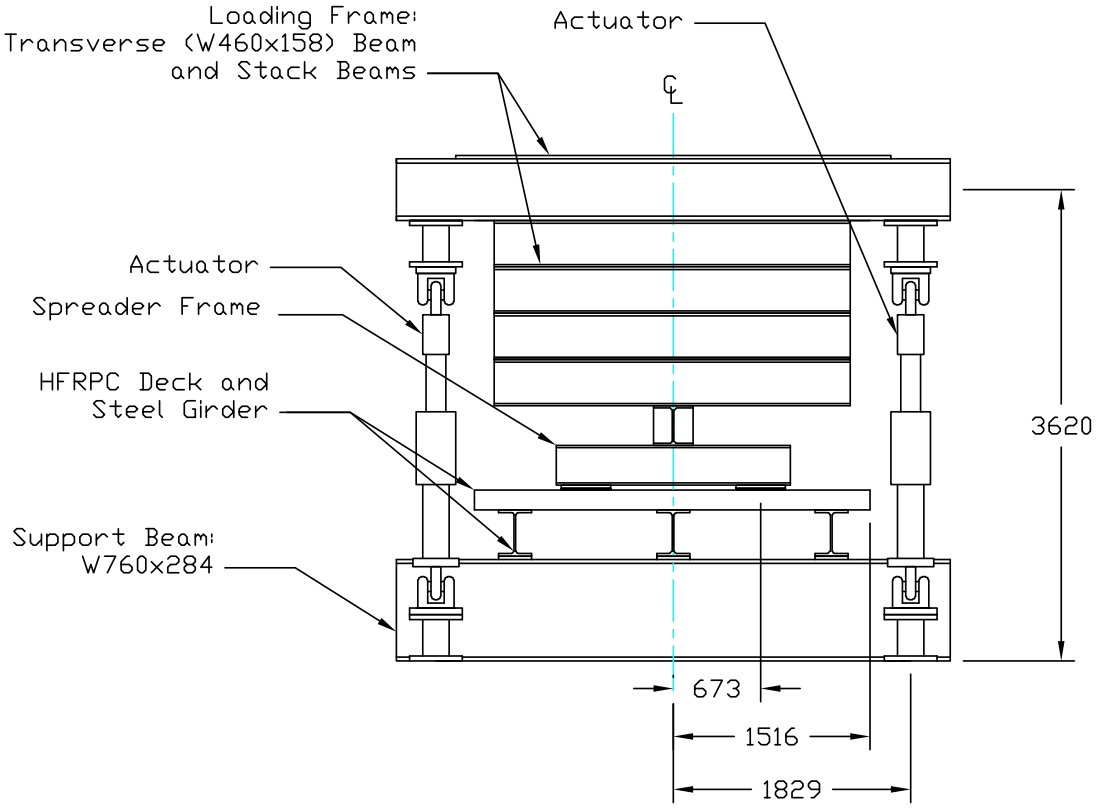

b. elevation

Fig. 5.2 Schematic showing destructive test setup (dimensions in mm)

5.3 Instrumentation

5.3.1 General

Various instruments and two data acquisition systems were used to measure and record the response of the HFRPC-SG specimen throughout the destructive test. The instrumentation layout for the destructive test differs from those used for the fatigue and creep testing in part due to the changed experimental setup and to avoid damaging instruments by not placing any beneath the HFRPC-SG specimen in the event of global collapse of the specimen, although judged unlikely given the lateral bracing and plastic capacity of the steel girders.

Table 5.1 provides a list of instruments including identification (ID), type, range and description of location on the specimen. The instrumentation for the destructive test includes: six ±50 mm linear variable displacement transducers (LVDT); two ±540 mm string potentiometers (String Pot.); four ±25 mm linear potentiometers (Linear Pot.); thirteen Krypton light emitting diodes (LEDs); twelve uni-axial strain gages; and uni-axial load cells and LVDTs housed in each of the two hydraulic actuators. The Krypton LEDs are part of a K600 Portable Coordinate Tracking and Measurement System (Krypton) manufactured by Krypton Industrial Metrology that is capable of measuring 3 translational degrees of freedom for a single LED and 6 (3 translational and 3 rotational) degrees of freedom with a minimum of three LEDs at a maximum sample rate of 3000 divided by the number of LEDs. The Krypton is a self-contained instrument and data acquisition systems that functioned independently of the other instruments and MEGADAC data acquisition system.

Table 5.1 List of Instruments

ID	Type	Range	Location
D1	LVDT	±50 mm	Top of center girder at south support
D2	LVDT	±50 mm	South-east load point on spreader frame
D3	LVDT	±50 mm	South-west load point on spreader frame
D4	LVDT	±50 mm	South-east load point on HFRPC deck
D5	LVDT	±50 mm	South side along center girder on HFRPC deck
D6	LVDT	±50 mm	South-west load point on HFRPC deck
D7	LVDT	±127 mm	LVDT housed in east actuator
D8	LVDT	±127 mm	LVDT housed in west actuator
D9	String Pot.	±540 mm	East side on loading frame
D10	String Pot.	±540 mm	West side on loading frame
D11	Linear Pot.	±25 mm	South-west steel-rubber pad
D12	Linear Pot.	±25 mm	South-east steel-rubber pad
D13	Linear Pot.	±25 mm	North-west steel-rubber pad
D14	Linear Pot.	±25 mm	North-east steel-rubber pad
D15	Krypton LED	N.A.	North face of spreader frame
D16	Krypton LED	N.A.	North face of spreader frame
D17	Krypton LED	N.A.	North-east load point on top flange of spreader beam
D18	Krypton LED	N.A.	North face of spreader beam on top flange
D19	Krypton LED	N.A.	North-west load point on top flange of spreader beam
D20	Krypton LED	N.A.	North-east load point on bottom flange of spreader beam
D21	Krypton LED	N.A.	North face of spreader beam on bottom flange
D22	Krypton LED	N.A.	North-west load point on top of steel-rubber pad
D23	Krypton LED	N.A.	South-east loading point on top flange of spreader beam
D24	Krypton LED	N.A.	South-west loading point on top flange of spreader beam
D25	Krypton LED	N.A.	North-west load point on bottom flange of spreader beam
D26	Krypton LED	N.A.	North side on HFRPC deck along interior girder
D27	Krypton LED	N.A.	South-west loading point on spreader frame at D3
S1	Strain Gage	±50000 μs	East girder centerline top flange
S2	Strain Gage	±50000 μs	East girder centerline web
S3	Strain Gage	±50000 μs	East girder centerline web
S4	Strain Gage	±50000 μs	East girder centerline bottom flange
S5	Strain Gage	±50000 μs	Center girder centerline top flange
S6	Strain Gage	±50000 μs	Center girder centerline web
S7	Strain Gage	±50000 μs	Center girder centerline web
S8	Strain Gage	±50000 μs	Center girder centerline bottom flange
S9	Strain Gage	±50000 μs	Center girder quarter-point top flange
S10	Strain Gage	±50000 μs	Center girder quarter-point web
S11	Strain Gage	±50000 μs	Center girder quarter-point web
S12	Strain Gage	±50000 μs	Center girder quarter-point bottom flange
F1	Load Cell	±448 kN	In-line with Actuator
F2	Load Cell	±448 kN	In-line with Actuator

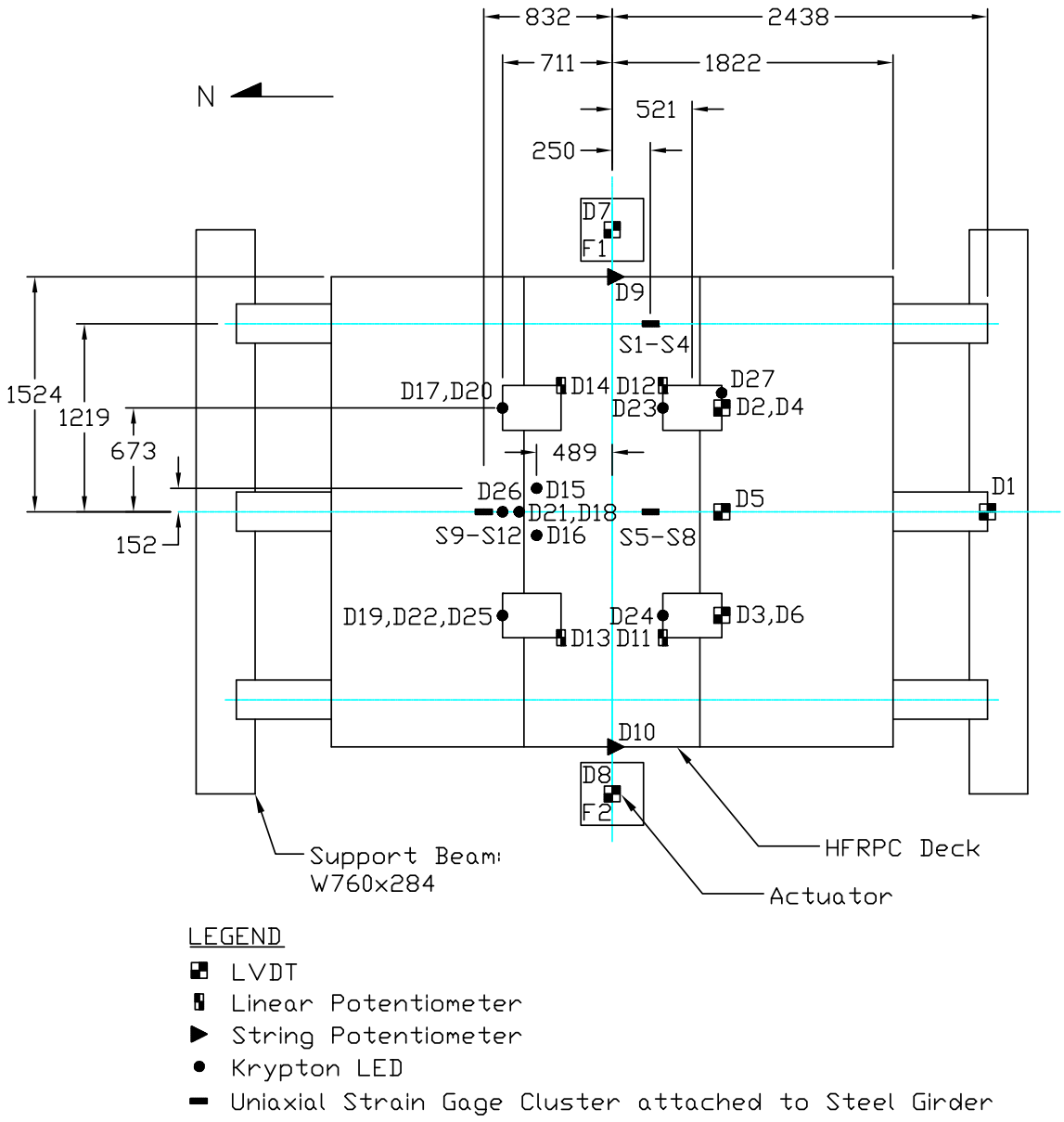

Fig. 5.3 Plan view of specimen showing instrumentation layout (dimensions in mm)

To account for the possibility of a time lag between the two data acquisition system, due to difference in the duration of time for each system to measure and digitize the information, a Krypton LED (D27) was placed at the same location of an LVDT (D3) so that the time lag could be quantified and data from one system could be time adjusted if necessary. Figure 5.3 presents the instrumentation layout for the destructive test shown on a plan view of the specimen including a legend and ID to identify the type and number of the instrument at a given location.

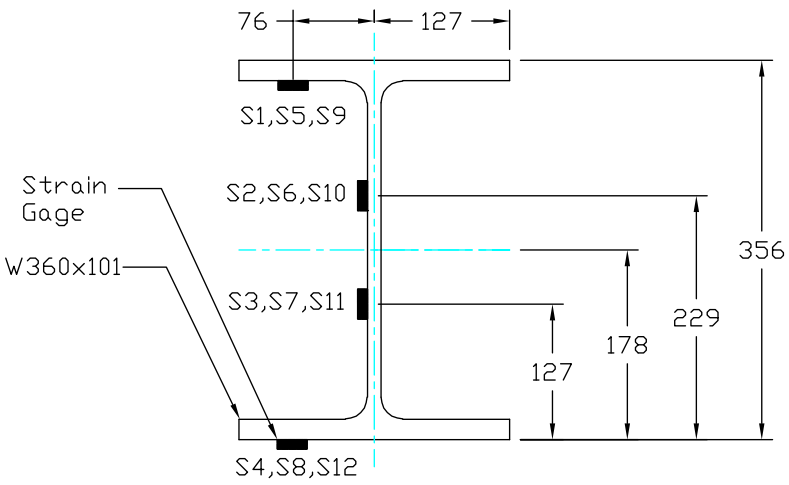

Fig. 5.4 Uniaxial strain gage cluster attached to steel girder (dimensions in mm)

Figure 5.4 presents the location of the individual uniaxial strain gages for each of the three strain gage clusters, specifically S1-S4 located at the approximate centerline of the east exterior girder, S5-S8 located at the approximate centerline of the interior girder and S9-S12 located approximately at the north quarter point of the HFRPC deck (see Fig. 5-3). Specifics pertaining to the placement of the instruments and data acquired are discussed in the subsequent sections.

5.3.2 HFRPC-SG Specimen

The global behavior of the HFRPC-SG system was monitored using a combination of LVDTs, Krypton LED and the actuator load cells. Vertical displacement of the HFRPC deck was measured at three locations along the interior girder, specifically, at the south support (LVDT: D1), 711 mm south of the HFRPC centerline (LVDT: D5) and 711 mm north of the HFRPC centerline (Krypton LED: D26). The LVDTs were installed on reference frames constructed over the HFRPC-SG specimen and attached to the HFPRC deck (D5) and interior steel girder (D1). Vertical displacement data from D5 and D26 was used to indirectly determine the vertical displacement at the centerline of the interior girder (a measure of the global response) that could not be measured without placing an instrument beneath the HFRPC specimen. Details regarding the calculation of the displacement at the center of the interior girder are discussed in the results section. The vertical force applied to the bridge specimen was measured and recorded via the two in-line uni-axial actuator load cell (F1 and F2). The load cell data (F1 and F2) in

conjunction with the calculated displacement at the center of the interior girder were used to plot the global force-displacement response of the HFRPC-SG specimen and to compare the global vertical stiffness with values obtained from fatigue testing to verify the indirect method.

Although not used to monitor the global behavior of the HFRPC-SG specimen, two string potentiometers (D9 and D10) were installed on the strong floor and attached to the loading frame to measure the vertical displacement and monitor the loading frame throughout the destructive test.

5.3.3 HFRPC Bridge Deck

The vertical displacement of the HFRPC deck was monitored at the four loading points using a combination of LVDTs, linear potentiometers and Krypton LEDs. At the south load points, the vertical displacements adjacent to the steel-rubber pads were measured using LVDTs (D4 and D6) mounted on a reference frame and attached to the HFRPC deck. At each of the north load points, the vertical displacement at a given point (either east or west) were determined by subtracting the displacement measured by the linear potentiometer (D13 on the west and D14 on the east) from the vertical displacement of the bottom flange of the spreader frame measured by the Krypton LEDs (D20 on the east and D25 on the west). This combination of instruments allowed the vertical displacement at each load point to be determined. Unfortunately without load cell at each point of loading the force transmitted through each location could not be determined. As a result, the local force-displacement behavior of the HFRPC deck could not be reported.

5.3.4 Composite Behavior

Strain gages installed at three locations (see Figs. 5.3 and 5.4) were used to measure and record longitudinal strain at various heights on the steel girders so that strain profiles could be used to determine and monitor the location of the neutral axis – an indicator of composite action between the HFRPC bridge deck and supporting steel girders. Two clusters of four uni-axial gages were installed approximately 250 mm south of the centerline of the interior (S5-S8) and east exterior girder (S1-S4) as illustrated in Fig. 5.3. The third cluster of four strain gages was installed approximately 832 mm north of the

centerline of the interior girder (S9-S12) corresponding to the approximate quarter pont of the HFRPC deck.

5.4 Experimental Protocol

The experimental protocol consists of subjecting the HFRPC-SG specimen to quasi-static monotonically increasing displacement via the hydraulic actuators to observe one or more limit states of the specimen with emphasis placed on the failure of the HFRPC deck. Using displacement control, the actuators displaced at a rate of 6.5×10^{-3} mm/s noting that this displacement does not directly translate into displacement of the HFRPC deck due to the elongation of bolts, compression of the loading frame and the steel-rubber pads. However supplemental instruments and indirect calculations, as described in the previous section, were used to determine displacements at the various locations. Load was monitored via the in-line load cells housed in each actuator. After the first limit state (failure mode) has been observed, displacement controlled loading will continue to be increased until it is judged no longer safe to continue with testing.

Load was applied to the HFRPC deck in a four point loading pattern via the hydraulic actuators, loading frame and spreader frame to simulate the AASTHO design tandem truck axle. The four points of loading were approximately centered between girders and equidistant from the center of the span (see Fig. 5.3).

5.5 Experimental Observations

5.5.1 General

This section describes, in chronological order, important observations made throughout the duration of the destructive test. Once initiated, the test could not be paused and for safety reasons close-up visual inspection could not be performed until the conclusion of the test. Therefore most of the observations described in this section are auditory observations that were occasionally accompanied by an apparent visual observation. Following the chronological list of observations a description of the post-test inspection accompanied by photographs is presented.

5.5.2 Chronological List

1. Approximately 2,000 seconds after initiating the destructive test with an applied load of 334 kN (2.7xTandem) cracking of the FRP deck was audible continuing intermittently thereafter.

2. At approximately 2,300 seconds with an applied load of 378 kN (3.1xTandem) continuous audible cracking was followed by a single noticeably louder cracking sound. Although difficult to determine the loud cracking sound appeared to have originated from the north-east point of loading.

3. At approximately 3,400 seconds with an applied load of 565 kN (4.6xTandem) continuous audible cracking was followed by a single noticeably louder cracking sound.

4. At approximately 4,300 seconds with an applied load of 703 kN (5.75xTandem) a series of loud cracking sounds and a series of bang noises indicative of the crushing of confined concrete. Again, although difficult to locate precisely the sounds appeared to have originated from the north-east point of loading.

5. At approximately 4,800 seconds with an applied load of 734 kN (6xTandem) continuous cracking sounds were followed by noticeably elevated cracking sounds.

6. At approximately 5,340 seconds with an applied load of 752 kN (6.1xTandem) two loud bangs were heard one after the other believed to originate from the north-east and south east loading points.

7. At 6,300 seconds with a load of 761 kN (6.2x Tandem) a series of loud bangs followed by failure at the north-east load point. The failure appeared to be a combination of punching-shear and web-buckling of the HFRPC deck as evidenced by the steel-rubber pad dropping into the HFRPC deck and rapid extension of the linear potentiometer (D14) at the north-east point of loading. A sudden drop in load followed the observed failure.

8. At 6,600 seconds and a load of 676 kN (5.5xTandem) a series of cracking sounds followed by a loud bang and failure of the south-east pad. Failure at the south-east pad appeared to be punching-shear noting that the steel-rubber pad appeared to remain above the HFRPC deck surface unlike the observed failure at the north-east location.

9. At 7,500 seconds and a load of 623 kN (5xTandem) significant rotation of the loading frame about the east-west axis was observed accompanied by severe twisting and rotation of the spreader frame about the north-south axis due to failure of the HFRPC bridge deck at the north-east location as shown by the photograph presented in Fig. 5.5.

10. At 8,200 seconds with a load of 645 kN (5.3xTandem) another loud bang sound from the north-east load point was heard and believed to be failure of the lower FRP flange. Sever rotation and twisting of the spreader frame was observed with bearing of the north east-west wide flange section of the spreader frame bearing on the HFRPC deck at the location of the interior girder. An increase in the applied load was observed and continued to the conclusion of the test.

Fig. 5.5 Photograph of spreader frame and failure at north-east load point

11. At 9,500 seconds with a load of 818 kN (6.7xTandem), the largest load achieved in the destructive test, an additional load bang noise was heard although the origin could not be determined.

12. At 9,900 seconds and approximately 800 kN (6.5xTandem) the destructive test was stopped due to concern for the safety of the equipment based on severe rotation of the loading frame about the east-west axis accompanied by severe rotation and twisting of the spreader frame.

5.5.3 Post-Test Inspection

Following the conclusion of the destructive test the loading frame and spreader frame were removed to facilitate post-test inspection of the HFRPC deck and steel girders. No noticeable global residual deformation was observed suggesting that the girders remained elastic or nearly elastic. The most notable failure occurred in the HFRPC deck at the north-east loading point were the rubber-steel pad punched through the HFRPC top flange into the HFRPC deck cavity as shown in the photographs presented in Fig. 5.6a and Fig. 5.6b. Figure 5.6a also shows the rubber-steel pads at the other three loading locations remained atop the HFRPC deck. Closer inspection revealed crushing of the concrete and failure of the inclined web at the north-east location over a length approximately equal to the width of the steel-rubber pad (250 mm) that is shown in the photograph presented in Fig. 5.6c. Further inspection of the underside of the HFRPC deck showed impending punching shear failure of the bottom FRP flange of the deck that is shown by photograph presented in Fig. 5.6d.

a. HFRPC deck surface

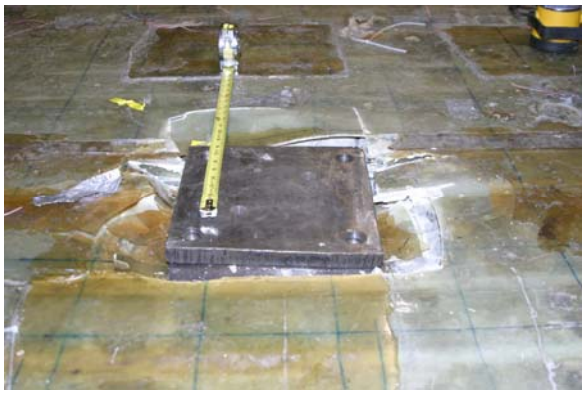

b. failure of deck at north-east location

c. failure of inclined web

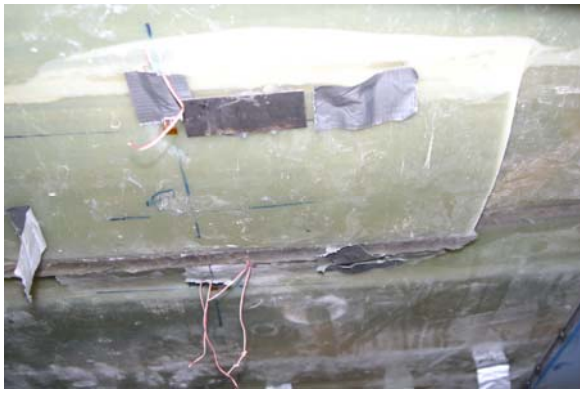

d. underside of HFRPC deck

Fig. 5.6 Photographs of HFRPC failure at north-east point of loading

Figure 5.7 presents photographs of the HFRPC deck surface at the four points of loading. With the exception of the north-east location (Fig. 5.6b), noticeable east-west cracks were observed at each of the other three locations with the most severe cracking observed at the south-east location. Although the top FRP layer of the HFRPC deck was not removed for inspection, likely significant crushing of the concrete in the top flange would have been observed at each location as suggested by the several loud audible “bang” sounds heard throughout the destructive test indicative of the crushing of confined concrete.

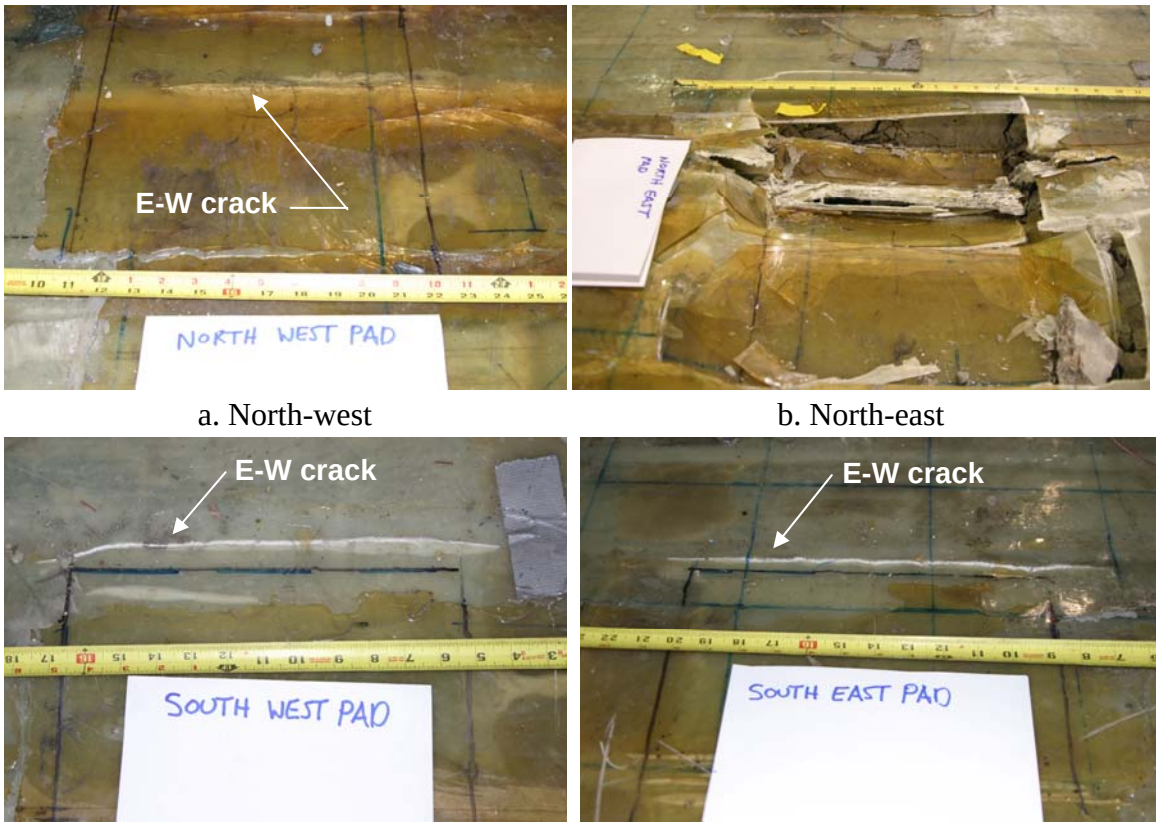

a. North-west b. North-east

c. South-west d. South-east

Fig. 5.7 Photographs of HFRPC deck surface at points of loading

5.6 Experimental Results

5.6.1 General

Data collected during the destructive test was used to determine the global force-displacement response of the HFRPC-SG specimen, the local vertical displacement response of the HFRPC deck at each of the four points of loading and to monitor the composite action between the supporting steel girders and the HFRPC deck.

The following sections present detailed descriptions of the determination of the global, local and composite action response of the HFRPC-SG specimen and corresponding results from destructive test.

5.6.2 HFRPC-SG Specimen

The applied load determined from actuator load cells (F1 and F2) and the vertical displacement at the center of the interior girder were used to characterize the global

response of the HFRPC-SG specimen. However, the vertical displacement at the center of the interior girder could not be measured directly due to the loading frame above the HFRPC deck and concern that instruments installed beneath the deck might be damaged during testing should the HFRPC-SG specimen collapse. Therefore vertical displacement data collected at two locations on the HFRPC bridge deck along the length of the interior girder (D5 and D26, see Fig. 5.3) were used to indirectly determine the vertical displacement at the center of the interior girder.

The vertical displacement at the center of the interior girder was determined using the Rayliegh-Ritz method whereby the deformed shape is assumed to take a polynomial form that could also be expressed as a trigonometric function To determine the vertical displacement at the center of the interior girder a third-order polynomial was used to approximate the deformed shape:

$$v(x) = a_1 x^3 + a_2 x^2 + a_3 x + a_4 \tag{5-1}$$

where $v(x)$ is the vertical displacement at location x and a_1, a_2, a_3 and a_4 are coefficients. Using Eq. 5-1, the boundary conditions [specifically $v(0) = 0$ and $v(L = 4826\,\text{mm}) = 0$] and displacement data from D26 and D5 located at 1727 mm and 3150 mm, respectively, the coefficients of the polynomial could be determined at each load step using the following system of equations:

$$0 = a_1 (0)^3 + a_2 (0)^2 + a_3 (0) + a_4 \tag{5-2}$$

$$0 = a_1 L^3 + a_2 L^2 + a_3 L + a_4 \tag{5-3}$$

$$v(x_{D5}) = a_1 {x_{D5}}^3 + a_2 {x_{D5}}^2 + a_3 x_{D5} + a_4 \tag{5-4}$$

$$v(x_{D26}) = a_1 {x_{D26}}^3 + a_2 {x_{D26}}^2 + a_3 x_{D26} + a_4 \tag{5-5}$$

where x_{D5} is the location of D5 with respect to the distance from the north support and equal to 3150 mm; x_{D26} is the location of D26 and equal to 1727 mm; $v(x_5)$ is the

vertical displacement at x_{D5} measured by D5 and $v(x_{26})$ is the vertical displacement at x_{D26} measured by D26. From Eq. 5-2 it is apparent that $a_4 = 0$. Expressing the system of equations (Eqs. 5-3, 5-4 and 5-5) in matrix format and solving for the coefficients yields:

$$\begin{bmatrix} a_1 \\ a_2 \\ a_3 \end{bmatrix} = \begin{bmatrix} L^3 & L^2 & L \\ x_{D5}^3 & x_{D5}^2 & x_{D5} \\ x_{D26}^3 & x_{D26}^2 & x_{D26} \end{bmatrix}^{-1} \begin{bmatrix} 0 \\ v(x_{D5}) \\ v(x_{D26}) \end{bmatrix} \tag{5-6}$$

With the coefficients determined from Eq. 5-6 and the displacement data from D5 and D26 the vertical displacement of the centerline could be calculated at each time step using Eq. 5-1 and $x = 2413\,\text{mm}$. Calculating the coefficients at each load step allows the above procedure to account for changes in the deformed shape through the destructive test due to redistribution of load that certainly occurred after the failure of the HFRPC deck at the north-east load point.

Figure 5.8 presents vertical load (Fig. 5.8a) and vertical displacement (Fig. 5.8b) data as a function of time. The vertical load presented in Fig. 5.8a has been normalized by the scaled tandem load (equal to 124 kN). Figure 5.8b presents displacement data from D5 and D26 along with the calculated displacement at the center (shown by a solid line). From Fig. 5.8 the load and vertical displacements are observed to increase approximately linearly up to an applied load of approximately 6 times the tandem load at 4,600 seconds corresponding to the onset of punching shear failure at the north-east point of loading. The load and displacement increased up to approximately 6.3 times the tandem load and a vertical displacement at the center of 11 mm at 6,000 seconds followed by a rapid drop in load corresponding to failure of the inclined FRP web at the north-east point of loading. Up to 6,000 seconds the vertical displacement at the center was larger than the vertical displacements at D5 and D26 however failure of the north-east pad lead to significant rotation of the spreader and loading frame that resulted in redistribution of load from 6,000 seconds to approximately 8,200 seconds as is evidenced by the divergence of the vertical displacements measured at D5 and D26 in this period of time. At approximately 8,000 seconds the north lateral beam of the spreader frame began bearing on the HFRPC deck directly over the interior girder as indicated by the increase

in applied load however the applied load was no longer being applied symmetrically to the HFRPC-SG specimen as is evidenced by the divergence of vertical displacements at D5 and D26 and the vertical displacement at D26 (located on the north side of the loading frame) beginning to exceed the vertical displacement at the center of the interior girder.

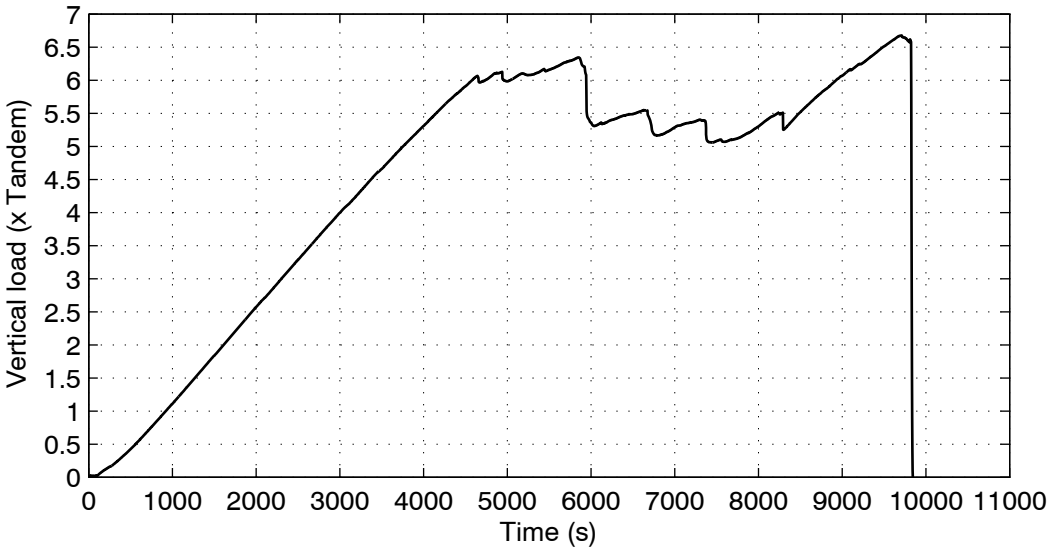

a. applied vertical load

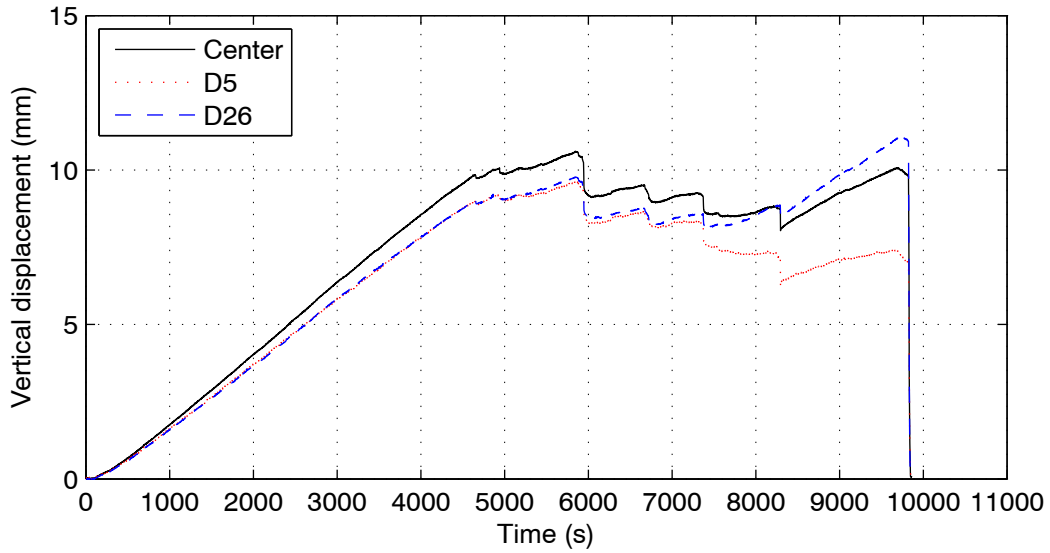

b. vertical displacement of HFRPC deck along interior girder

Fig. 5.8 Applied load and vertical displacement results of HFRPC-SG specimen

To verify the Rayleigh-Ritz method was generating reasonable deformed shapes, i.e. shapes that conform to the boundary conditions and specified displacements, the deformed shape profile of the interior girder was plotted for two load levels, specifically 3 and 6 times the tandem load. Figure 5.9 presents the deformed shape for 3 and 6 times the tandem load determined using the Rayleigh-Ritz method shown by solid and dashed lines respectively along with vertical displacement data from D5 and D26 shown by an x-shaped marker and a circle marker. The profiles plotted in Fig. 5.9 indicate that the Rayleigh-Ritz method appears to have provided reasonable estimates based on the zero displacement boundary conditions and the agreement between the measured and calculated displacements at the D5 and D26 locations as would be expected. Further verification of the Rayleigh-Ritz method is provided in the subsequent section when the elastic stiffness of the HFRPC-SG specimen determined from destructive testing is compared with the elastic stiffness determined from fatigue testing (see Section 4) where the vertical displacement of the center of the interior girder was measured directly.

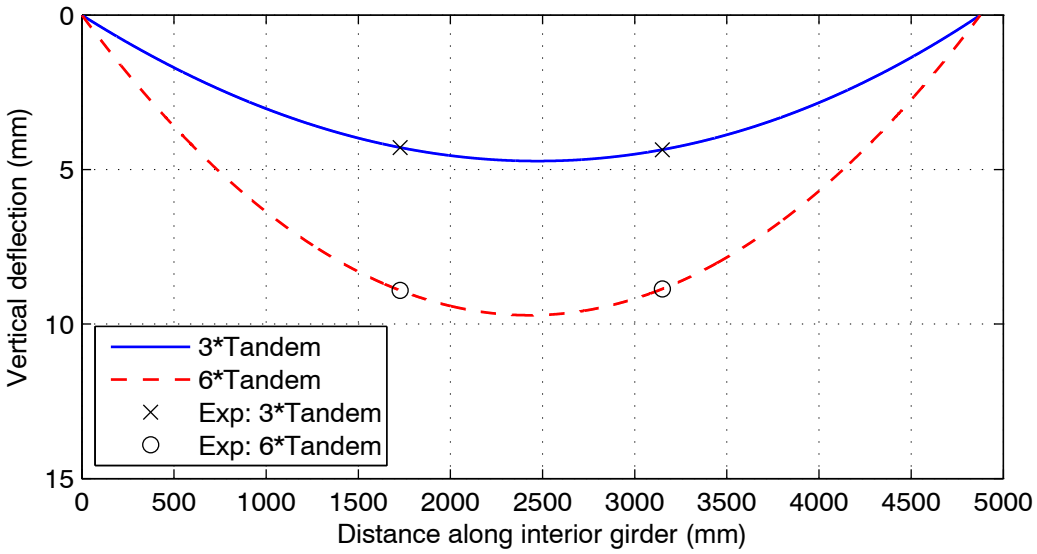

Fig. 5.9 Deformed shape of the interior girder

The global force-displacement response of the HFRPC-SG specimen determined from the load cell data (F1 and F2) and the calculated vertical displacement at the center of the interior girder is presented in Fig. 5.10. Figure 5.10a presents a plot of the complete force-displacement response of the HFRPC-SG specimen however following failure of the HFRPC deck at the north-east location there was a redistribution of loading resulting in decreasing vertical displacement at the center of the interior girder obscuring the results. Figure 5.10b presents the force-displacement response up to just after failure of the HFRPC deck at the north-east location. From Fig. 5.10b the force displacement response is approximately linear up to 727 kN (5.9xTandem) and a vertical displacement of 9.7 mm. After this point the force-displacement response becomes nonlinear continuing to increase to a load of 764 kN (6.25xTandem) and a vertical displacement of 10.5 mm at which point the inclined web of the HFRPC deck at the north-east load point failed resulting in a drop in load and recovery of a portion of the total vertical displacement. Figure 5.10c presents the force-displacement response over the range of load that was applied during the fatigue testing portion of the experimental study. From Fig. 5.10c the force-displacement response again appears linear, or nearly linear, with an applied load of 74 kN at a vertical displacement of 1 mm corresponding to a vertical stiffness of 74 kN/mm. This value agrees very well with the average vertical stiffness of 73.2 kN/mm determined from the static benchmark tests performed through the fatigue testing program (see Section 4) using displacement data measured directly at the center of the interior girder. The close agreement between the vertical stiffness from fatigue testing and destructive testing further suggest that the Rayleigh-Ritz method was a reasonable approach to indirectly determining the vertical displacement at the center of the interior girder.

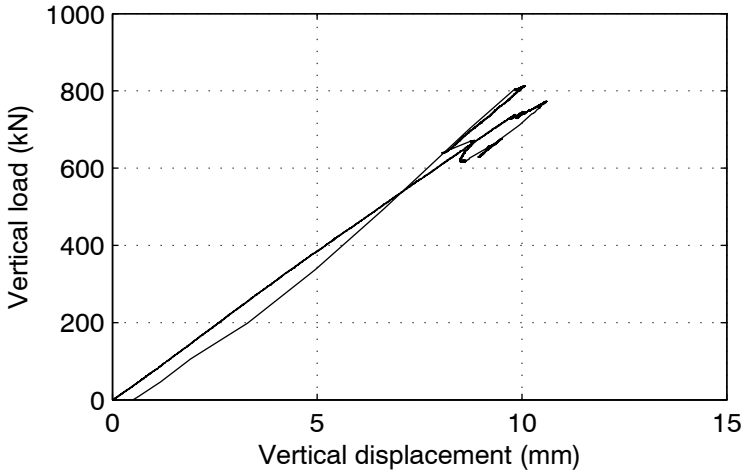

a. complete response

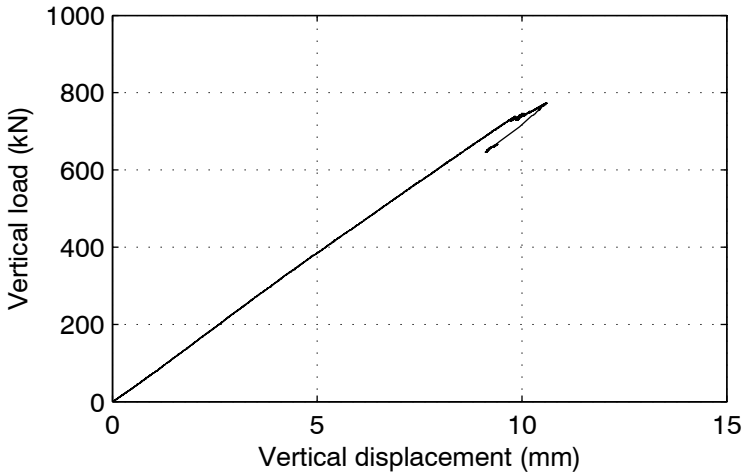

b. response up to failure

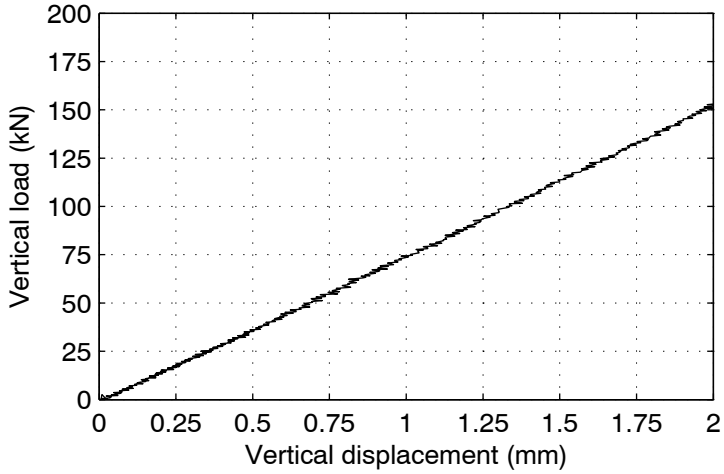

b. elastic response

Fig. 5.10 Force-displacement response of the HFRPC-SG specimen

5.6.3 HFRPC Bridge Deck

The existing experimental setup utilized for destructive testing was not designed to accommodate load cells placed at each of the four points of loading and consequently the load transmitted to each of the four locations on the HFRPC deck could not be determined. Therefore the primary data pertaining to the local behavior of the HFRPC deck that was collected and reported is the vertical displacement of the deck at the four locations of loading.

At the south-east and south-west points of loading the vertical displacement of the HFRPC deck was measured adjacent to the steel-rubber pad directly using LVDTs (D4 and D6, respectively) mounted on a reference frame and attached to the HFRPC deck surface. At the north-east and north-west loading locations the vertical displacement of the HFRPC deck adjacent to the steel-rubber pads was determined by subtracting the deformations across the elastomeric pad measured by linear potentiometers (D14 and D13, respectively) from the vertical displacement of the bottom flange of the lateral beam of the spreader frame measured using the Krypton Portable Measuring Machine and LEDs (D25 and D20, respectively).

Figure 5.11 presents the total applied load, normalized by the scaled tandem load of 124 kN, (Fig. 5.11a) and the vertical displacement of the HFRPC deck at the four points of loading (Fig. 5.11b) for the duration of the test. From the data presented in Fig. 5.11, the vertical displacements at each of the locations compare reasonable well up to approximately 2,000 seconds where the rate of vertical displacement of at the north-east (denoted NE) reduces while the vertical displacement at the other locations remain similar. The change in vertical displacement at the NE location at 2,000 seconds corresponds to the initiation of cracking as described in the Experimental Observations section. Although the rate of vertical displacement had slowed between 2,000 seconds and approximately 4,800 seconds, the applied load continued to increase in a reasonable linear manner up to 6 times the tandem load at approximately 4,800 seconds. At which point the applied load no longer increases linearly accompanied by a large increase in the vertical displacement at the NE location from approximately 7 mm at 4,800 seconds to 50 mm just prior to 6,000 seconds. At, 6,000 seconds, the vertical displacement increased

further, accompanied by a rapid drop in the applied load, as a result of the failure of the HFRPC deck at the NE location. The rapid increase in vertical displacement at the NE location at 6,000 seconds is due to crushing of the FPR inclined web allowing the steel-rubber pad and loading frame to punch into the HFRPC deck cavity and does not reflect the actual vertical displacement of the HFRPC deck at this point.

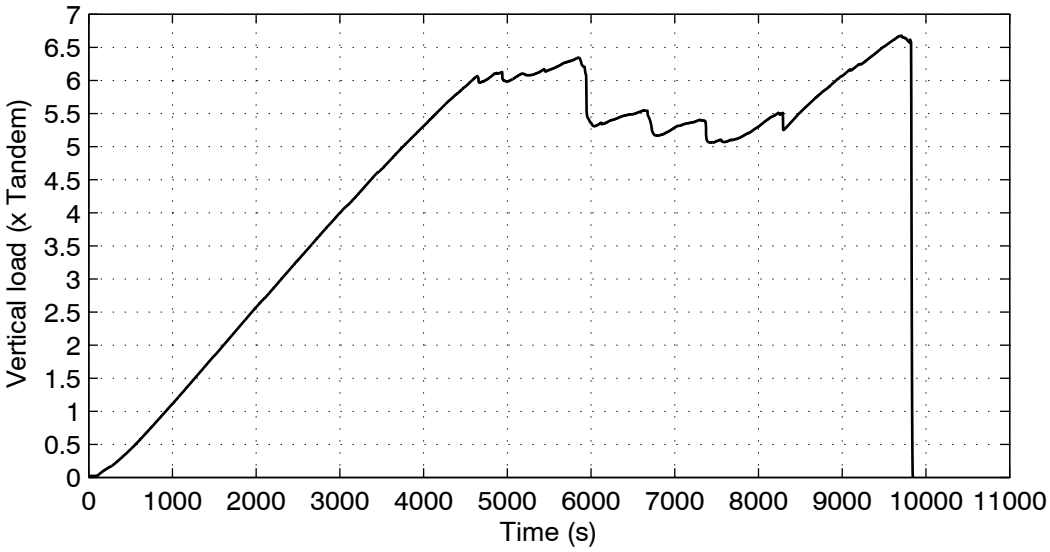

a. applied vertical load

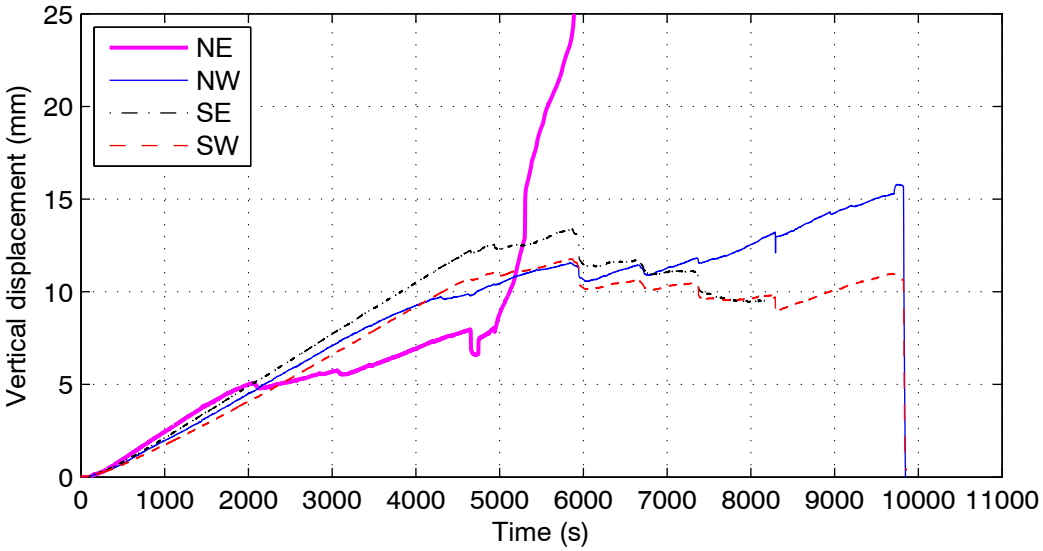

b. vertical displacement of HFRPC deck

Fig. 5.11 Applied load and vertical displacement results of HFRPC deck

5.6.4 Composite Behavior

The composite action between the HFRPC deck and steel girders was monitored using the position of the bending neutral axis at three locations. The neutral axis location was determined using longitudinal strain data from the strain gage sets installed at two locations on the interior (S5-S8 and S9-12 see Fig. 5.3) and exterior (S1-S4) girders collected throughout the destructive test. Figure 5.12 presents strain profiles for the approximate centerline of the interior girder (Fig. 5.12a), approximate quarter point of the HFRPC deck (Fig. 5.12b) and approximate centerline of the east exterior girder (Fig. 5.12c) for applied load levels of 1.0, 3.0, 6.0 and 6.6 times the scaled tandem load. Each plot in Fig. 5.12 presents the longitudinal strain, in units of micro-strain (μ), plotted at four different heights of the (W360x101) girder section (see Fig. 5.4) presented as the height of the gage normalized by the depth of the section ($d = 356\text{mm}$). From Fig. 5.12a, for each applied load level (up to 6.6 times the tandem representing the maximum applied load) each strain profile passes through zero strain at an approximate normalized height of 0.56 -representing the position of the neutral axis. These results suggest that composite action between the HFRPC deck and steel girder was present (indicated by position of the neutral axis that is greater than $0.5d$) and that the composite action at this location (approximate center of interior girder) was maintained at an applied load of 6.6 times the scaled tandem load. Also shown by the results presented in Fig. 5.12b is that the section remained elastic since all strain values were less than the expected yield strain of $2070\,\mu$: assuming a yield strength of 414 MPa and a Young's modulus of 200 GPa. Similar results are shown in Fig. 5.12b for the approximate quarter point of the HFRPC deck where the strain profiles pass through a value of zero strain at a normalized height of approximately $0.56d$ indicating that composite action was maintained throughout the destructive test at this location and that the section remained elastic with all strain values less than the expected yield strain. Although the malfunction of S1 at the approximate centerline of the east exterior girder prevents plotting the full profile the results that were obtained seem to agree with the other locations in that composite action was present and maintained through the test and that the section at this location remained elastic.

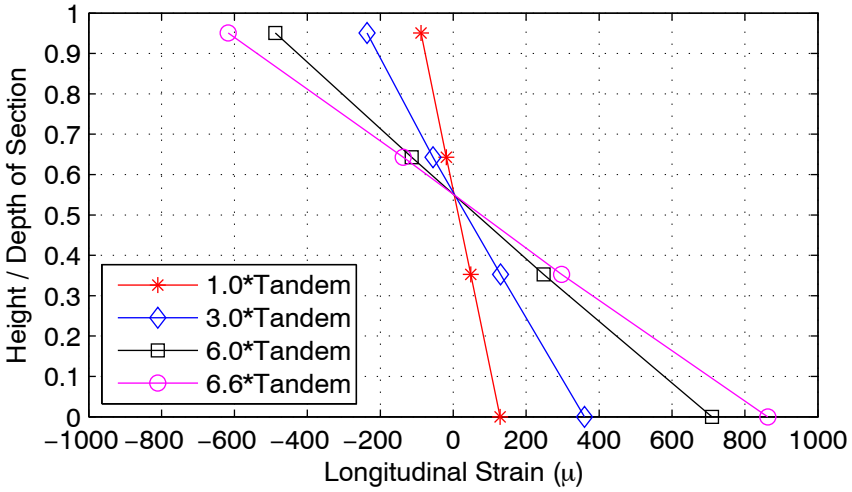

a. Centerline of interior girder

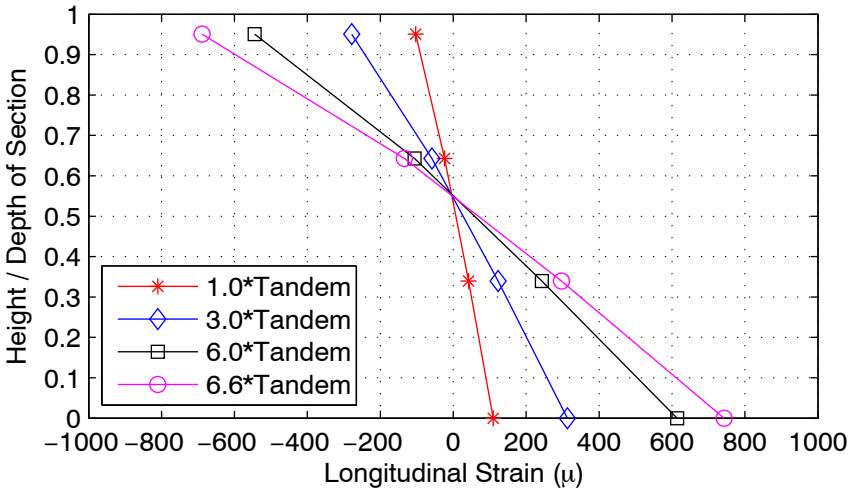

b. Quarter point of interior girder

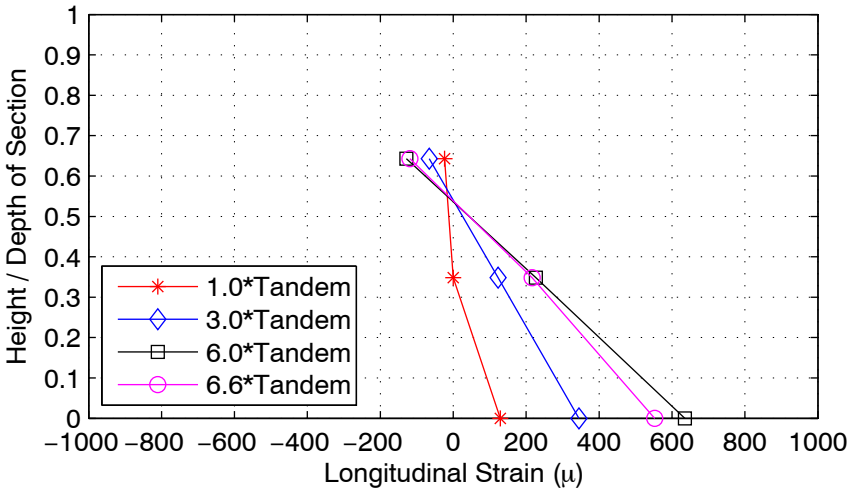

e. Centerline of east exterior girder

Fig. 5.12 Strain profiles across girders at various locations

SECTION 6

SUMMARY AND CONCLUSIONS

6.1 General

This report presented the results of an experimental investigation of the long term and ultimate behavior of a hybrid FRP-Concrete (HFRPC) deck and steel girder (HFRPC-SG) system. The experimental investigation included creep and fatigue testing to gain an improved understanding of the long term behavior of the hybrid-composite system and destructive testing to identify the failure mode and capacity of the HFRPC deck. The following sections provide a summary of the various components of the experimental investigation and conclusions drawn from the results of the individual tests.

6.2 Summary

To determine the creep behavior of the HFRPC deck and steel girder system the HFRPC-SG specimen was subjected to a sustained load of 114 kN (approximately equal to the scaled tandem load of 124 kN) for 51 days after which the load was removed and the recovery of the system was monitored. From the results of the creep test, creep deformations on the order of 18 to 20 percent of the initial static deformations were observed in the HFRPC deck that is likely due to creep of the concrete in the compression flange of the FRP deck. The results also showed that no creep was detected in the steel girders indicating that the creep behavior of the HFRPC deck was localized and did not affect the behavior of the global HFRPC-SG system. Upon removal of the load, approximately, 98 percent of the maximum displacement of the HFRPC deck and 100 percent of the vertical displacement in the steel girders was recovered after 21 days.

Fatigue testing consisted of subjecting the HFRPC-SG specimen to approximately 2 million cycles of dynamic loading with amplitude of 1.26 times the scaled tandem load (156 kN) over 35 nonconsecutive days performing static benchmark tests at 200,000 cycle intervals. Results of the static benchmark tests were used to determine the global stiffness of the HFRPC-SG specimen, local stiffness of the HFRPC deck at the four

points of loading and the position of the bending neutral axis in the steel girders – an indication of composite action between the HFRPC deck and supporting steel girders. The results of the static benchmark tests showed no degradation in the global stiffness, local stiffness or composite action of the HFRPC-SG specimen after 2 million cycles.

Destructive testing was performed to determine the capacity and failure mode of the HFRPC deck. The test consisted of subjecting the HFRPC-SG specimen to monotonically increasing vertical displacement while monitoring the applied load, displacement at various locations, and strain at three locations on the steel girders. Results from the destructive test showed the HFRPC deck sustained vertical load up to 2.7 times the scaled tandem load (330 kN) without damage. However at 2.7 times the scaled tandem load the FRP deck at the north-east location began cracking that continued to a load of 6.3 times the tandem load (771 kN) at which point the inclined web of the FPR deck crushed resulting in complete failure of the HFRPC deck at that location. Observations during the test and a post-test inspection reviled cracking at the other three points of loading and likely crushing of concrete based on the loud “bang” sounds heard throughout the test. Strain data obtained from the destructive test indicated no loss of composite action between the HFPRC deck and supporting steel girders even up to the maximum load of 6.6 times the scaled tandem load (820 kN).

6.3 Conclusions

The HFRPC deck acting compositely with steel girders exhibited excellent long term structural performance. The following are some of the distinct conclusions:

1. The creep performance is mainly influenced by the concrete portion of the section and the observed creep deformations were fully recovered after 21 days of the removal of the loading. Given that the nature of the loads applied to the HFRPC deck are transient and not stationary (traffic loading), the observed creep is not a limiting factor to the application of this concept as a replacement to concrete decks.

2. The HFRPC deck showed no degradation to stiffness and the specimen retained significant strength after fatigue loading. Moreover, the partial composite action between the steel girders and the HFRPC deck was not altered after the two million cycles. Therefore, the concept of clustering shear studs might provide a valid approach of connecting FRP decks to steel girders.

3. Clearly, the ultimate capacity of HFRPC deck exceeded the design expectations. With the HFRPC deck reaching approximately 3 times the tandem load without damage clearly indicates the robustness of the HFRPC deck design concept and its validity to be used in actual bridges to replace concrete decks.

REFERENCES

American Association of State Highway and Transportation Officials, (1998), *AASHTO LRFD Bridge Design Specifications*, Second Edition, AASHTO, Washington, D.C.

Alnahhal, W., Aref, A. and Alampalli, S. (2008). "Composite Behavior of Hybrid FRP-Concrete Bridge Decks on Steel Girders." Journal of Composite Structures, Vol. 84/1 29-43.

Alnahhal, W. I. (2007), Structural Characteristics and Failure Prediction of Hybrid FRP-Concrete Bridge Superstructure and Deck Systems, Ph.D. Dissertation, the State University of New York, University at Buffalo.

Aref, A. J. (1997), A Novel Fiber Reinforced Composite Bridge Structural system, Ph.D. Dissertation, the University of Illinois at Urbana-Champaign.

Aref, A.J. and Alnahhal, W. I. (2006), Hybrid FRP-Concrete Bridge Deck Systems: Development and System Performance Validation", Technical No. C-02-07, New York State Department of Transportation, Albany, New York.

Ashby, M. F. (1991), "Overview No.92 – Materials and Shape", *Acta Metallurgica et Materialia*, Vol. 39, No. 6, pp. 1025-1039.

Bakeri, P. A., and Sunder, S. S. (1990), "Concepts for Hybrid FRP Bridge Deck Systems," *Serviceability and Durability of Construction Materials*, Proceedings of the First Materials Engineering Congress, Denver, Colorado, August 13-15, 1990, ASCE, Vol. 2, pp. 1006-1015.

Busel, J. P., Editor (2000), Product Selection Guide: FRP Composite Products for Bridge Applications, First Edition, The Market Development Alliance of the FRP Composites Industry, Harrison, NY.

Federal Highway Administration and Federal Transit Administration (FHWA) (2003), 2003 Status of the Nation's Highways, Bridges and Transit: Conditions and Performance-Report to Congress, http://www.fhwa.dot.gov/policy/2002cpr/report .htm [Oct.0 3. 03].

Kitane, Y. and Aref, A. (2004), "Static and fatigue testing of hybrid fiber-reinforced polymer-concrete bridge superstructure", *Journal of Composites for Construction*, Vol. 8, No. 2, pp. 182-190.

Lesko, J. J., Hayes, M. D., Schniepp, T. J. and Case, S. W. (2001), "Characterization and durability of FRP structural shapes and materials", *Composites in Construction: A reality*, pp. 110-120.

Market Development Alliance of the FRP Composites Industry (2002), Industry Overview: Overview of the FRP Composites Industry – A Historical Perspective, Market Development Alliance of the FRP Composites Industry, http://www.mada composites.org /Industry_Overview.htm [Dec.03.02].

Mirmiran, A., Shahawy, M., and Beitleman, T. (2001), "Slenderness limit for hybrid FRP-concrete columns," *Journal of Composites for Construction*, Vol. 5, No. 1, pp. 26-34.

Moon, FL., Eckel, DA., Gillespie, JW. (2002), "Shear Stud Connection for the Development of Composite Action between Steel Girders and Fiber Reinforced Polymer Bridge Decks", *Journal of Structural Engineering*, Vol. 128, No. 6, pp. 762-770

Reising, R., Shahrooz, B., Hunt, V., Neumann, A., Helmicki, A. and Hastak, M. (2004), "Close Look at Construction Issues And Performance of Four Fiber-Reinforced Polymer Composite Bridge Decks", *Journal of Composites for Construction*, Vol. 8, No. 1, pp. 33-42.

Righman, J., Barth, K. and Davalos, J. (2004), "Development of an efficient connector system for fiber reinforced polymer bridge decks to steel girders", *Journal of Composites for Construction*, Vol. 8, No. 4, pp. 279-288.

Seible, F., Karbhari, V. M., Burgueño, R., and Seaberg, E. (1998), “Modular advanced composite bridge systems for short and medium span bridges,” *Developments in Short and Medium Span Bridge Engineering '98*; Proc., 5th Int. Conf. on Short and Medium Span Bridges, Calgary, Canada, Canadian Society of Civil Engineers, CD-ROM, 431–441.

Zetterberg, T., Astrom, B. T., Backund, J. and Burman, M. (2001), “On Design of Joints between Composite Profiles for Bridge Deck Applications”, *Composite Structures,* Vol. 51, pp. 83-91.

Zhou, A. and Keller, T. (2005), “Joining techniques for fiber reinforced polymer composite bridge deck systems”, *Composite Structures*, Vol. 69, No. 3, pp. 336-345.